General Disclaimer

One or more of the Following Statements may affect this Document

- This document has been reproduced from the best copy furnished by the organizational source. It is being released in the interest of making available as much information as possible.

- This document may contain data, which exceeds the sheet parameters. It was furnished in this condition by the organizational source and is the best copy available.

- This document may contain tone-on-tone or color graphs, charts and/or pictures, which have been reproduced in black and white.

- This document is paginated as submitted by the original source.

- Portions of this document are not fully legible due to the historical nature of some of the material. However, it is the best reproduction available from the original submission.

FINAL REPORT

FOR

RADIANT COOLER DESIGN AND EMISSIVITY STUDY

PART I

RADIANT COOLER DESIGN

(8 APRIL 1969 - 31 OCTOBER 1969)

CONTRACT NO.: NAS5-11683

Prepared by

ITT Aerospace/Optical Division

Fort Wayne, Indiana 46803

For

Goddard Space Flight Center

Greenbelt, Maryland 20771

FINAL REPORT

FOR

RADIANT COOLER DESIGN AND EMISSIVITY STUDY

PART I

RADIANT COOLER DESIGN

(8 APRIL 1969 - 31 OCTOBER 1969)

CONTRACT NO.: NAS5-11683

Goddard Space Flight Center

Contracting Officer: Newchy Mignone

Technical Monitor: Dr. Warren A. Hovis 622

Prepared by

ITT Aerospace/Optical Division
Fort Wayne, Indiana 46803

Project Manager: Richard V. Annable

For

Goddard Space Flight Center
Greenbelt, Maryland 20771

ABSTRACT

This part of the report covers the design and thermal analysis of a single stage radiant cooler for operation from one side of a Nimbus spacecraft. The cooler is designed to attain a temperature in the 30 K to 100 K range at a minimum altitude of 500 n mi and a maximum base temperature of 35 C over the range of orbital plane to earth-sun line angles from 0 degrees to 15 degrees. Reasonable but relatively large changes in the thermal parameters of the design do not produce correspondingly large changes in the cooler temperatures. The thermal analysis of the radiant cooler is based on techniques employing the specular image model. These techniques are generally applicable to the design and analysis of any radiant cooler with rectangular geometry.

The second part of the report covers a study of the emissivity of cone wall materials.

TABLE OF CONTENTS

LIST OF ILLUSTRATIONS

LIST OF TABLES

1.0 INTRODUCTION

This report describes the design and thermal analysis of a single stage radiant cooler which views cold space from a single side of a spacecraft. The cooler is designed to operate on a Nimbus satellite in a near polar, sun-synchronous orbit. Its maximum patch (detector) temperature is to be in the range from 95K to 100K under the following worst conditions:

a. Minimum spacecraft altitude of 500 nautical miles.

b. Maximum orbit plane to earth-sun line angle of 15 degrees.

c. Maximum base temperature of 35 C.

These conditions plus additional constraints are used to establish a range of radiant cooler designs (Section 2.0). A specific example (design II) from this range is selected and analyzed in detail (Section 3.0). Finally variations are made in the selected design in order to improve its performance, and one variation (modified design II) is also analyzed in detail (Section 4.0).

In order to attain the required patch temperature in a single stage radiant cooler, it is necessary to shade the cone top (cone end and cone mouth) from direct sunlight and to have a relatively large ratio of cone end area to cone mouth area (i.e., more than half low α/ϵ surface at the cone top). The sun shading does not have to be complete, however, because the same shield also provides a partial shading from earth radiation. In addition, the view angle from the patch to cold space away from the earth is increased to include a small view of the solar panel. The resultant temperature rise in the patch is less than 1 K (Section 3.4).

The increased view to cold space reduces the cone-patch radiative coupling (effective patch-to-cone emissivity). The cone-patch coupling is also reduced by insulating the sides, as well as the bottom, of the patch from the cone structure by means of multilayer insulation. Only the black top of the patch radiates to cold space. The addition of multilayer insulation to the sides also reduces the radiative input through the optical openings (Appendix I).

The requirements of the statement of work for a single stage radiant cooler are very nearly met by design II (Sections 2.0 and 3.0). Only at the worst sun angle (15 degrees) and the maximum anticipated effective cone wall emissivity (0.07) does the patch temperature exceed the 100K limit, and then by less than 1 K. A more realistic set of worst conditions (at the same minimum spacecraft altitude and maximum base temperature) are a 12 degrees sun angle and a cone wall emissivity of 0.05. In this case the patch temperature is reduced by about 6K. Use of modified design II (Section 4.0) provides an additional reduction of approximately 3K. The patch temperature is then safely below the 100K limit for all orbit and cone wall conditions.

The analytic techniques developed on this program (Section 5.0 and 6.0) are generally applicable to the design and analysis of a radiant cooler of rectangular geometry (i.e., one in which the cone cross section perpendicular to the patch normal is a rectangle). The basis of the techniques is the multiple specular image model. The assumption of specular reflection at the cone walls yields a conservative (worst case) result for the cone temperature. This is so because specular reflection generally maximizes the absorption of incident external radiant power (E. M. Sparrow and R. D. Cess, Radiation Heat Transfer, Brooks/Cole, 1966, pp. 163-169). The only exception is when the cavity effect vanishes. This occurs for large cone angles when incident parallel rays only partially irradiate the cone mouth (E. M. Sparrow and S. H. Lin, Absorption of Thermal Radiation in V-Groove cavities, U. of Minn. for NASA/Lewis, N62 10682, July 1962). On the other hand, specular reflection at the cone walls minimizes the cone-patch radiative coupling for a given value of cone wall (hemispherical) emissivity. In addition, deviations from specular reflection at the cone walls may return patch radiation to the patch after one or more reflections.

An example of the importance of the effective (i.e., including the influence of deviations from specular reflection) specular cone wall emissivity is given in Section 3.2 A decrease from 0.07 to 0.05 produces a reduction in patch temperature of about the same amount as the modification to design II. Although the reductions may be important, in neither case are they a very large percentage of the patch temperature (only about 3 percent). This is an illustration of the fact that reasonable changes in a radiant cooler design (i.e., to its thermal properties or geometry) do not produce large changes in patch temperature. Significant changes in cooler performance require major alterations to the basic design approach. This is illustrated above by the departures from earlier designs needed to attain a patch temperature of 100K or less in a single stage Nimbus radiant cooler.

Nevertheless, the present uncertainty in the effective cone wall emissitivity and the resultant variations in patch temperature are sufficiently large to warrant a study of cone wall materials. This is the subject of the second part of the program, covered in Part II of the Final Report.

2.0 RANGE OF DESIGNS

It is assumed that the radiant cooler has a rectangular geometry in which the patch normal (cone axis) is parallel to the orbit normal and the plane of the cone mouth is parallel to that of the patch. A range of rectangular radiant cooler designs was subjected to a set of conditions or constraints. The basic conditions are those imposed by the Statement of Work:

a. Minimum spacecraft aititude of 500 n mi.

b. Orbit plane to earth-sun line angle of 0 degrees to $\pm$ 15 degrees (sun-synchronous).

c. Cooler base (instrument) temperature range of 5 C to 35 C.

The first two conditions were translated into requirements on the earthward view to cold space and on the direct sunlight shading of the cone mouth.

(1) Maximum view angle to cold space in the vertical plane through the centers of the patch and earth of 28 degrees toward the earth.

(2) No direct sunlight in the cone mouth for sun angles from 0 degrees to 12 degrees.

At the minimum altitude of 500 n mi, the earth (radius of 3444 n mi) and its atmosphere (9.1 n mi tropopause) at the equator begin at an angle of 29 degrees and 8 minutes below a horizontal plane. An additional angle of about 1 degree was subtracted to allow for spacecraft wobble.

The thermal analysis in Sections 3.0 and 4.0 show that an increase in direct sunlight is not desirable. There is a rapid increase in temperatures as the sun angle increases from 12 degrees to 15 degrees. On the other hand, the temperatures are nearly constant for sun angles from 0 degrees to 12 degrees, the approximate range experienced by Nimbus I, II, and III. Therefore, a reduction in direct sunlight exposure is not necessary either, and condition (2) is a good one.

The view angle to cold space away from the earth in the vertical plane was also restricted in order to limit the view factor from the patch to the solar panel to a very small value.

(3) Maximum view angle to cold space in the vertical plane of 50 degrees away from the earth.

The condition was based on the assumption that the solar panel is the same as that on Nimbus D. Rather than prevent the patch from seeing the solar panel altogether, it is better to allow a small view of the panel and therefore a larger upward view angle

to cold space. The larger view angle decreases the cone wall absorption of external radiation (i.e., the number of cone wall reflections necessary for an external ray to leave the cone mouth) as well as the radiative coupling from cone to patch (i.e., the number of cone wall reflections necessary for a patch ray to reach cold space). Moreover, the increased view angle reduces the cone length needed for a given patch width or enlarges the patch width for a given cone length. (First Quarterly Report on Contract NAS5-10113, May, 1966, Appendix I).

Any increase in the view angle to above 50 degrees is limited not only by the rapidly increasing view of the solar panel but also by the spacecraft structure that generally lies above the radiant cooler. A decrease produces a trade-off between the increased cone-patch radiative coupling and cone wall absorption of external radiation and an increased patch or cone end area.

The following conditions were imposed in order to keep the cone-patch radiative coupling at a low value. It is possible to meet them because of the relatively large view of cold space available in three directions.

(4) No more than one cone wall reflection to cold space for rays leaving the patch in the horizontal plane and away from the earth in the vertical plane.

These conditions keep the fraction of rays requiring three cone wall reflections at a negligible value (Appendix III). They therefore also simplify the analysis of the cone-patch radiative interchange. The same trade-off discussed for condition (3) exists when conditions (4) are relaxed to permit an increase in the number of cone wall reflections for patch rays traveling to cold space.

The patch radiating (black) area should be sufficiently large that the thermal inputs resulting from the introduction of the infrared detectors (joule heat, lead conduction, radiative input through the optical openings) produce an acceptably small temperature rise in the patch. We have therefore imposed the following condition.

(5) Minimum area at the patch opening (cone cross-section at the plane of the patch top) of 3.2 square inches.

At a temperature of 95K, the temperature rise produced by a thermal input of 2 mw in a patch 3 square inches radiating area is about 5K. Since the detector thermal inputs are expected to be somewhat higher, either the initial patch temperature must be smaller or the patch area larger. The problem is to obtain a sufficient patch area in a radiant cooler that meets all the other conditions.

Finally, we imposed a condition reflecting the limited space available for the radiant cooler.

(6) Maximum linear cooler dimension of 12 inches.

For a given patch area, the patch width required to meet the other conditions imposed on the design increases as the maximum linear dimension decreases.

All conditions except number (1) are somewhat arbitrary. In general, however, conditions along the lines of those stated above are imposed on any cooler design.

The cooler designs were initially carried out by means of scale drawings, starting with the patch opening (black patch area plus patch-cone clearance area). A minimum opening width of 0.80 inch was selected to allow for mounting the detector package and the last focusing lens within this dimension. The following designs covered are listed in Table 1.

Table 1
Range of Radiant Cooler Designs

Design	Patch Opening Width * a	Length * b
I	0.80	4
II	1.00	3.2
III	1.20	2.66
IV	1.40	2.28
V	1.60	2.00
VI	1.80	1.78
VII	2.00	1.60

* In Inches

In order to meet conditions (1) and (4), the cone wall angle (with respect to the patch normal or cone axis) for the upper (anti-earthward) wall must be 31 degrees or larger. Lower vertical cone wall angles of 10 degrees, 15 degrees, and 20 degrees were considered. The 10 degree value was taken as a practical lower limit.

The designs meeting conditions (1) through (6) are listed in Table 2. All have lower vertical cone wall angles of 10 degrees. The upper vertical cone wall angle is 32 degrees and 55 minutes in all cases, while the horizontal cone wall angle varies from 17 degrees to 25 degrees. All designs are identical in the vertical plane except for a scale factor.

Table 2
Range of Designs Meeting Conditions

Design	Patch Opening Width a	Length b
II	1.00	3.20
III	1.20	3.34

Table 2 (Cont.)
Range of Designs Meeting Conditions

Design	Patch Opening Width a	Length b
IV	1.40	2.86
V	1.60	2.50
VI	1.80	2.22

Designs I and VII could not simultaneously meet all conditions. Specifically, if all other conditions were met, condition (2) was not. Design II could not meet all conditions at the larger patch opening length of 4 inches.

Once the patch area (opening) has been fixed, the conductive inputs are set by the electrical leads required and by the support needed to survive the vibration environment. The radiation entering from the optical openings may be considered a fixed input (Appendix I) together with the joule heating of the detectors. The remaining thermal input to the patch is then the radiation from the cone walls. To minimize this, both the cone temperature and cone-patch radiative coupling must be minimized. The cone-patch coupling is least for the largest b/a ratio. The cone temperature is least for the greatest earth shielding, least cone wall cavity absorption of external ratiation, and largest cone end to cone mouth area ratio. With the given set of conditions, all these factors are also optimum at the largest b/a ratio. Everything except the patch area therefore points to design II as the optimum subject to the imposed conditions.

However, an increase in the maximum linear dimension would permit all conditions to be met with the larger patch length (4 inches) in design II or with design I. The b/a ratio would thereby be increased and the thermal performance improved. Conversely, a reduction in the maximum linear dimension would require the use of a higher numbered design (III and above). This would lower the b/a ratio and degrade the thermal performance.

By design, sun shielding of the cone top does not vary significantly among the designs. Also, the radiative input to the cone end from the low-emissivity shield is relatively small in all cases.

2.1 Design II

The exact geometry of radiant cooler design II is shown in Figure 1, 2, and 3. The patch dimensions are those of the cone opening at the top of the patch and therefore include the cone-patch clearances. Similarly, the dimensions of the cone top (cone end and cone mouth) include the end-shield clearances.

For a vertical plane patch dimension of 1.00 inch and a lower vertical plane cone wall angle of 10 degrees, the upper cone wall angle is 32 degrees and 55 minutes

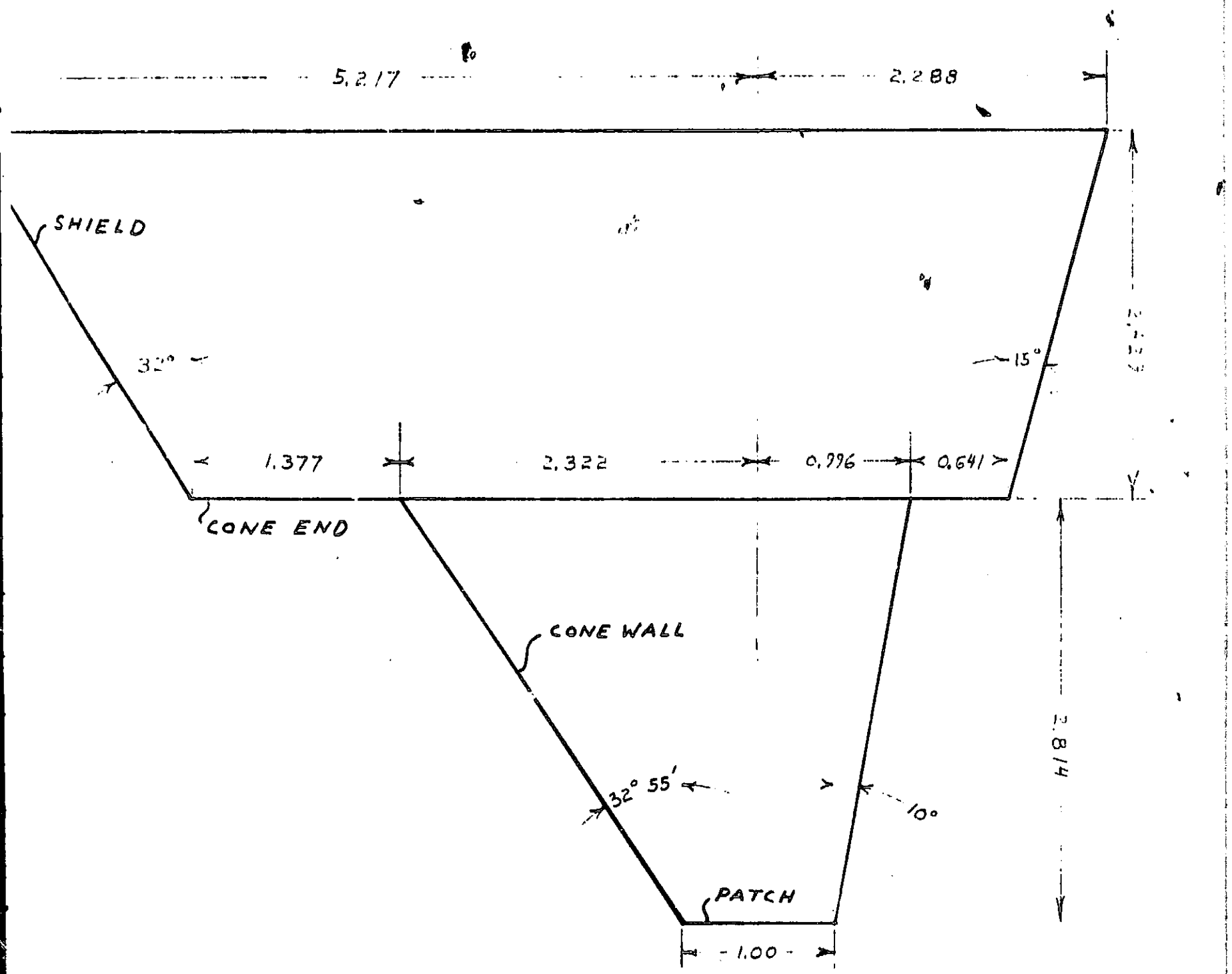

Figure 1 Vertical Plane of Design II

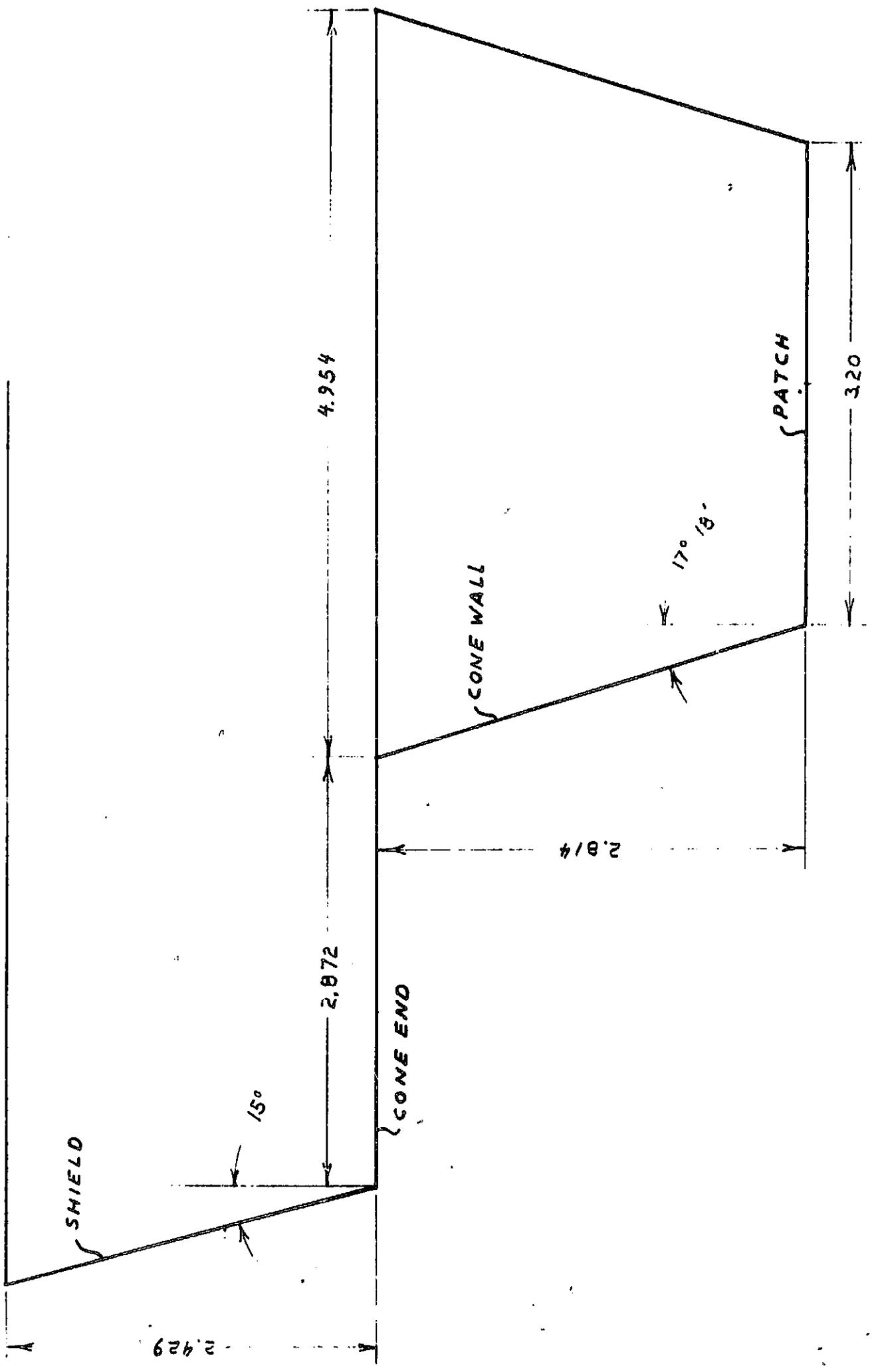

Figure 2 Horizontal Plane of Design II

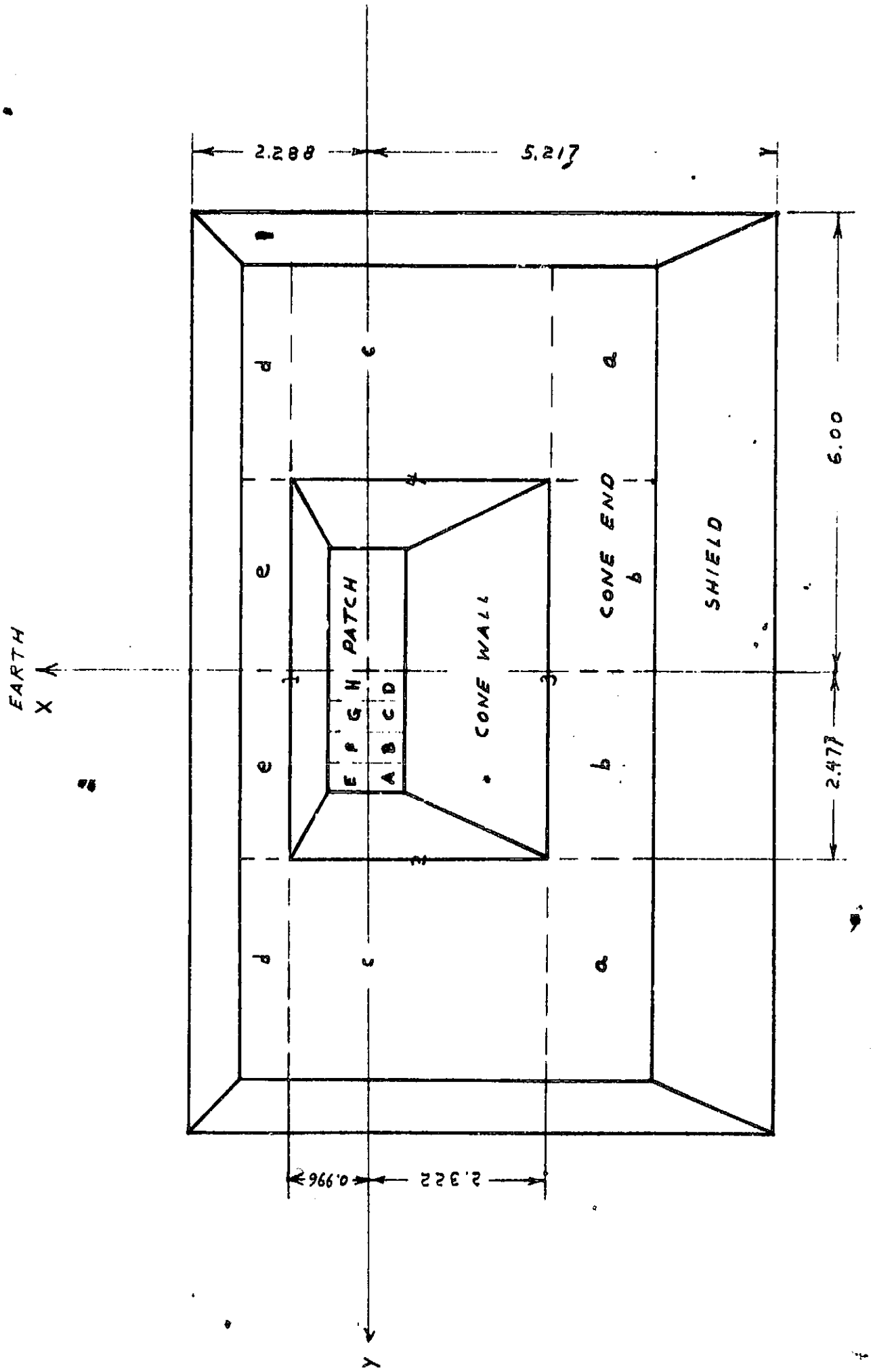

Figure 3 Top View of Design II

for an upward patch view angle of 50 degrees. These same factors also determine the cone length (2.814 inches) and cone mouth dimension (3.318 inches).

The condition that no more than one cone wall reflection is needed for a horizontal patch ray to reach cold space determines the condition on the horizontal angle θ_H,

$$\frac{\sin 2\,\theta_H}{\ell c \sec \theta_H} = \frac{\cos 3\,\theta_H}{W_H}$$

Where ℓc = cone length
W_H = patch dimension in horizontal plane

Solving for θ_H, we obtain

$$\tan \theta_H = \frac{-1 + \sqrt{3a^2 + 1}}{3a}$$

where $a = \ell c / W_H$. For design II, $a = 0.8794$ and

$$\tan \theta_H = 0.3116$$

$$\theta_H = 17 \text{ degrees and } 18 \text{ minutes}$$

The height of the shield is then determined in the horizontal plane by the requirement that it not be seen by the patch and by the condition of a maximum linear dimension of 12 inches. For design II, the shield extends 2.429 inches above the plane of the cone top. The patch opening and cone wall angle also determine the cone mouth dimension and thereby complete the geometry in the horizontal plane.

The shield angle was set at 32 degrees in the vertical plane away from the earth so that the cone end cannot see the earth by reflection in this shield (This requires a minimum angle of 31 degrees). The remaining shield angles were set at 15 degrees (i.e., normal incidence for direct solars rays at the maximum sun angle), so that scattering off the shield to the cone top is negligible.

Given the shield angles and the shield height, the vertical plane design was completed by requiring the top rim of the shield to coincide with the extreme rays from the patch (i.e., the rays at the maximum patch look angles) in the directions toward and away from the earth. This condition provides maximum shielding of the cone top while meeting the requirement that the patch not see the shield. At the same time, it provides the minimum vertical plane dimension (subject to all the imposed conditions). On the other hand, the area of the cone end could be increased by allowing the vertical plane dimension to approach its maximum allowable value of 12 inches with a consequent reduction in shielding of the cone top.

2.2 Design III

The exact geometry of radiant cooler Design III is shown in Figures 4, 5, and 6. The trends as one goes from design II to designs III and IV are for the cone-patch radiative coupling to increase and for the cone temperature to increase. The cone temperature increases as a result of the reduced shielding of the earth, the increased cone wall absorptivity of external radiation, and the reduced cone end to cone mouth area ratio. These trends are offset, at least in part, by a decrease in the shield radiative input to the cone end and by the increased patch area. The increased patch area reduces the influence of the fixed thermal inputs which result from introduction of the detectors (bias heat and radiative inputs through the optical openings).

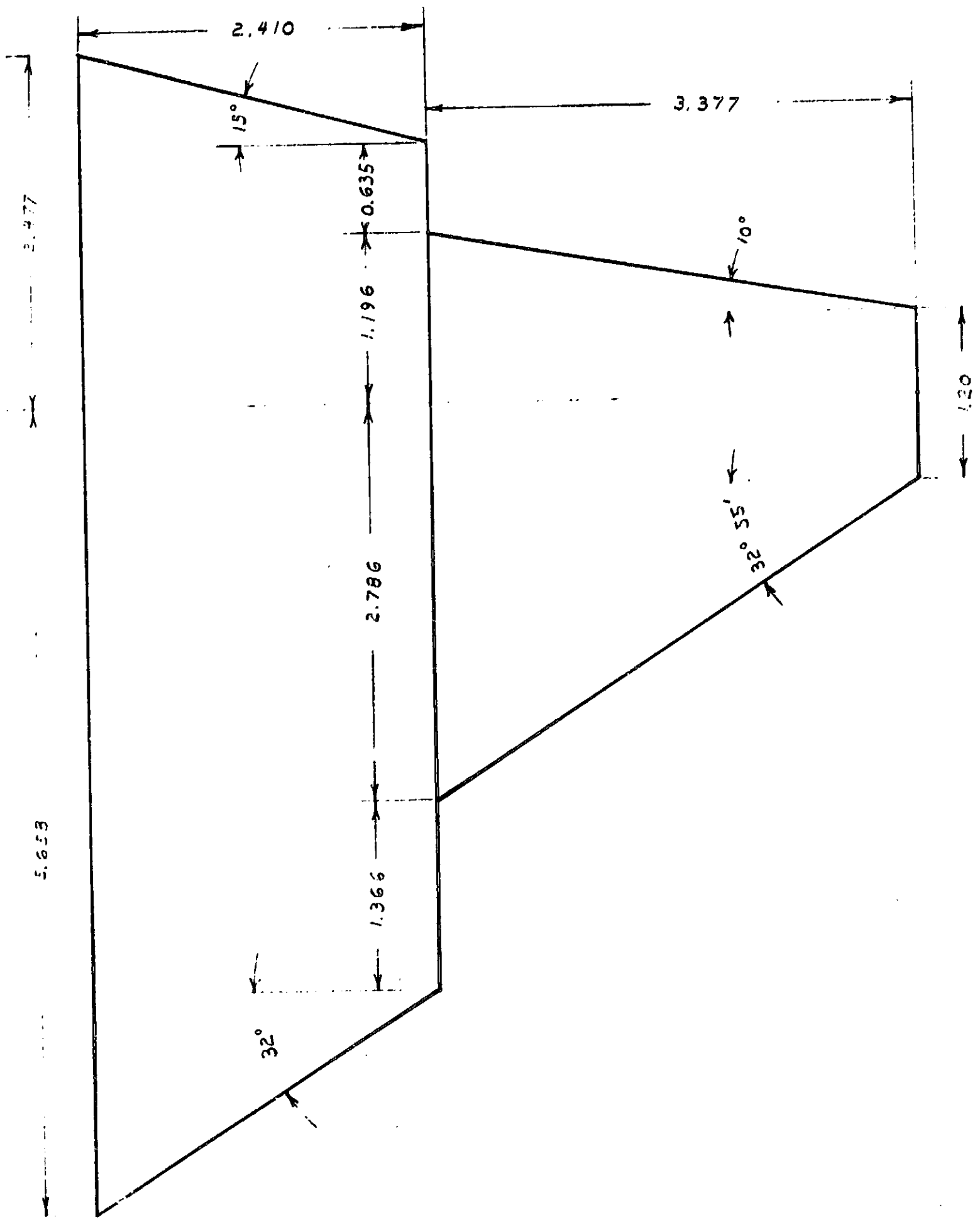

Figure 4 Vertical Plane of Design III

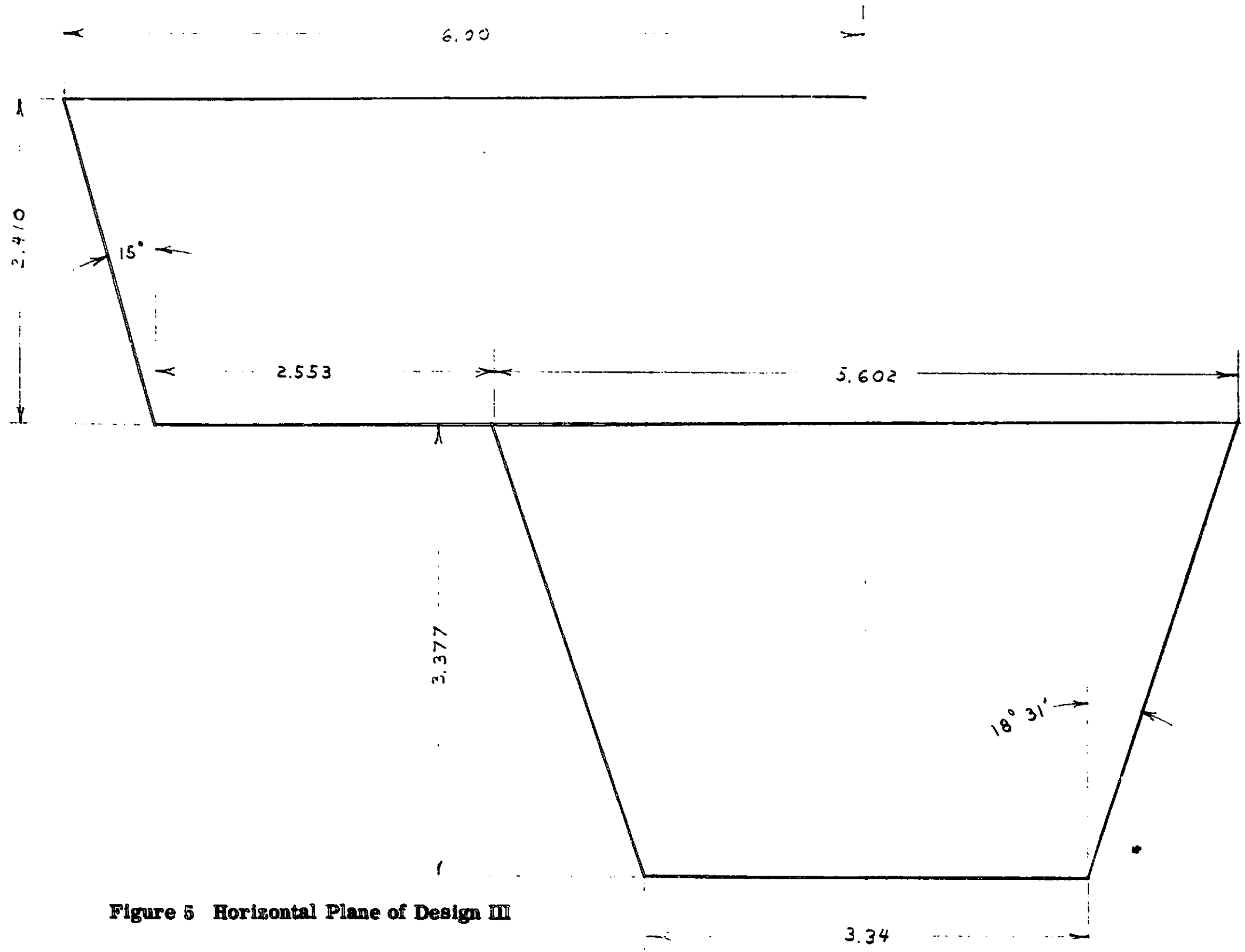

Figure 5 Horizontal Plane of Design III

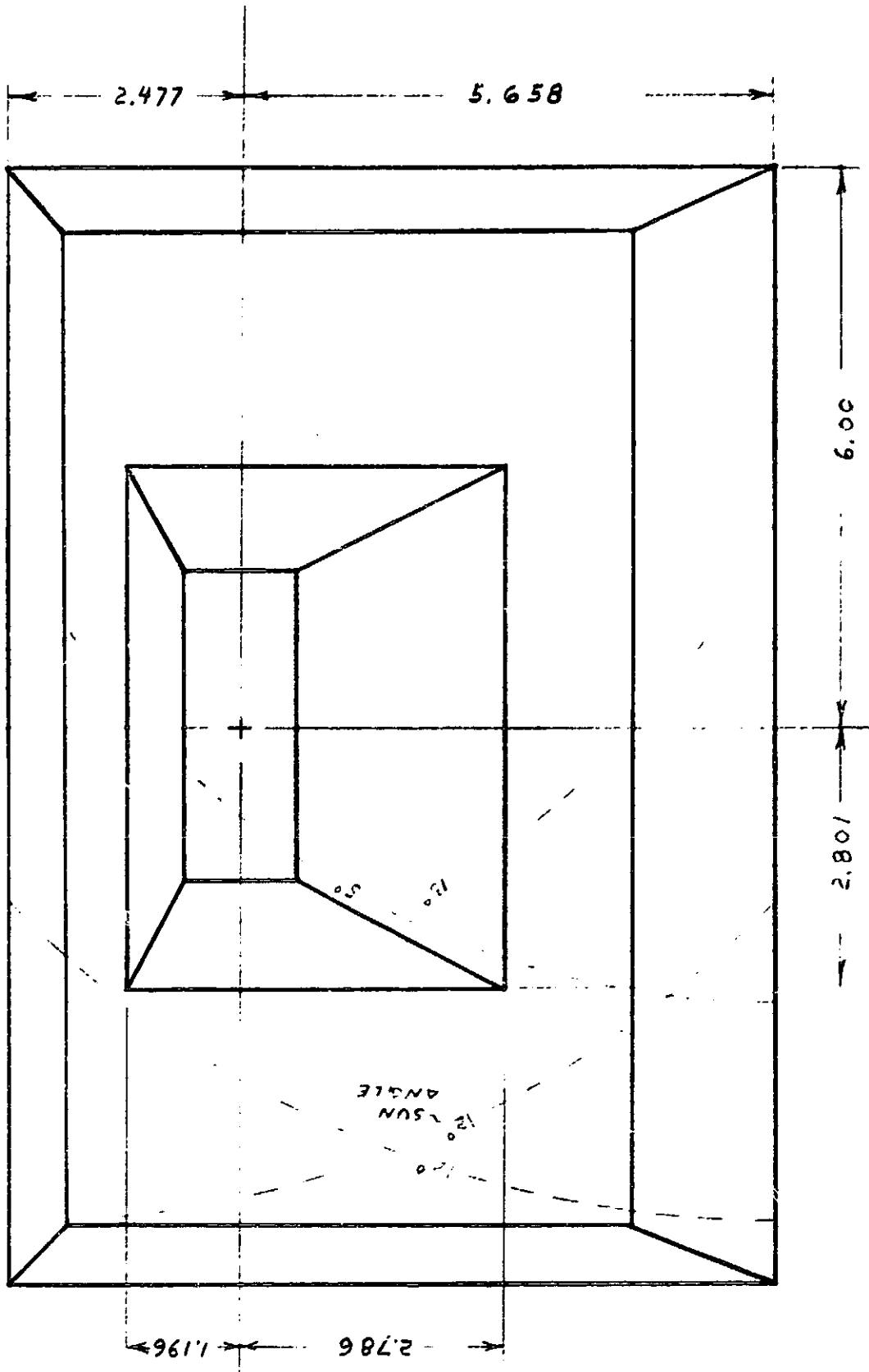

Figure 6 Top View of Design III

3.0 THERMAL ANALYSIS OF DESIGN II

The techniques for the thermal analysis of a rectangular radiant cooler are developed in Sections 5.0 and 6.0 and used to calculate the radiative transfer parameters for design II. These results are applied below to the calculation of the cone and patch temperatures in design II. The analysis is carried out for three sun angles (0 degrees, 12 degrees, 15 degrees) and for two values of effective cone wall emissivity (0.05 and 0.07).

The cone temperature varies from 166.4 K at a sun angle of 0 degrees to 166.9 K at 12 degrees and 175.1 K at 15 degrees. Variations in the number of cone supports show that the conductive input to the cone has only a small influence on the temperature. Larger temperature changes result from comparable variations in the cone end to cone mouth area ratio.

The patch temperature for a cone wall emissivity of 0.07 varies from 97.9 K to 98.0 K and 100.8 K as the sun angle goes from 0 degrees to 12 degrees and 15 degrees. The corresponding temperatures for a cone wall emissivity of 0.05 are 94.5 K, 94.8 K, and 97.3 K. Comparable changes in patch temperature are produced by the same percentage changes in the radiative input, conductive input, and detector input.

Two conclusions are apparent. First, the patch temperature in design II is nearly constant for sun angles of 12 degrees and less. And secondly, reasonable variations in the thermal parameters do not produce large changes in the temperatures. This is especially true of the cone. And in the patch, a $\pm$ 25 percent variation in the detector (electrical and optical) thermal input of 2.4×10^{-3} W produces a change in patch temperature of only $\pm$ 1.5 percent. Moreover, a 40 percent increase in the effective cone wall emissivity (from 0.05 to 0.07) results in a patch temperature increase of only 3.5 percent.

It should be mentioned, however, that temperature changes of these magnitudes may be of importance in obtaining improvements in infrared detector performance.

Finally, it is shown that the solar panel produces only a small temperature rise ($\sim$ 0.6 K) in the patch of design II. The improved performance anticipated from an enlarged upper view from the patch (condition 3 in Section 2.0) can therefore be realized.

3.1 Cone Temperature Range

The thermal balance equation of the cone is

$$\epsilon_d \sigma T_c^4 = (1/A_d) \bar{\Phi}_r + (1/A_d) \bar{\Phi}_k, \qquad (1)$$

where T_c = cone temperature

ϵ_d = emissivity of cone end

A_d = area of cone end

Φ_r = radiative input from earth, shield, and direct sunlight

Φ_k = conductive input from instrument housing (base)

The radiative input is given by

$$\frac{1}{A_d} = [\alpha_{me} W_r + \epsilon_{me} W_e + \alpha_{ms} \cdot S_o \cdot \sin \beta_s] \frac{A_m}{A_d} + \epsilon_d \, a_{dh} \, \sigma T_h^4 + (\alpha_d W_r + \epsilon_d W_e) F_{de} + \alpha_d \cdot g_d \cdot S_o \cdot \sin \beta_s \quad , \qquad (2)$$

where W_r = average reflected sunlight exitance of earth

W_e = average infrared exitance of earth

S_o = solar constant ($0.14 \ W_{cm}^{-2}$)

α_{me} = effective cone mouth absorptivity for earth reflected sunlight

ϵ_{me} = effective cone mouth absorptivity for earth infrared

α_{ms} = effective cone mouth absorptivity for direct sunlight

β_s = solar elevation angle above plane of the cone top

A_m/A_d = ratio of cone mouth area to cone end area

a_{dh} = effective emissivity of the shield as seen from the cone end

α_d = solar absorptivity of cone end

T_h = temperature of instrument housing

F_{de} = view factor from cone end to earth

g_d = solar exposure factor for cone end .

The terms multiplied by A_m/A_d apply to the cone mouth (i.e., the cone walls) and the remaining terms to the cone end. The equation neglects the cone mouth absorption of shield (infrared) radiation and the cone mouth emission of (infrared) radiation, which are small and tend to offset each other. In addition, the shield is assumed to be at the temperature of the instrument housing.

From Appendix I to Part I of the Final Report on Contract Number NAS5-10113 (December 1967), we have

$$W_e = 2.1 \times 10^{-2} \text{ W cm}^{-2}$$

$$W_r = \frac{1}{2\pi} S_o A \frac{\sin^2 \vartheta_o}{1 - \cos \vartheta_o} \cdot \cos \beta_s \quad , \qquad (3)$$

where A is the average solar reflection factor for the earth (0.4) and $\pi/2 - \vartheta_o$ the nadir to earth tangent line angle. At an altitude of 500 nautical miles, ϑ_o is 29 degrees 8 minutes, and

$$W_r = 1.67 \times 10^{-2} \cdot \cos \beta_s \ W_{cm}^{-2} \quad .$$

The emissivity ϵ_d of a good white paint is 0.85 and its solar absorptivity α_d, 0.25. The infrared absorptivity ϵ_c of a gold coated cone wall is assumed to be 0.05 and its solar absorptivity α_c, 0.22. Using the results given in Sections 5.0 and 6.0, we can calculate the effective absorptivities. The results are listed in Table 3.

Table 3

Effective Absorptivities of Design II

$$\alpha_{me} = 0.0359$$

$$\epsilon_{me} = 0.008935$$

$$\alpha_{ms} = \begin{cases} 0, & \beta_s = 0^o \\ 0, & \beta_s = 12^o \\ 1.4 \times 10^{-3}, & \beta_s = 15^o \end{cases}$$

$$a_{dh} = 1.688 \times 10^{-2}$$

The area ratio A_m/A_d is 1/2.47 for design II, and the maximum housing temperature T_h is 35C (308K). The view factor F_{de} is 0.0961, (Section 5.0) and the solar exposure factor g_d is 0.86×10^{-2} at β_s = 12 degrees and 9.61×10^{-2} at β_s = 15 degrees (Section 6.0). The resultant radiative inputs to the cone per unit of cone end area are listed in Table 4 for solar elevation angles of 0 degrees, 12 degrees, and 15 degrees.

Table 4

Cone Radiative Inputs per Unit of Cone End Area

β_s	$\frac{1}{A_d} \Phi_r$ (W_{cm}^{-2})
0^o	3.168×10^{-3}
12^o	3.231×10^{-3}
15^o	4.034×10^{-3}

The conductive input from the instrument housing to the cone is given by

$$\Phi_K = K_c (T_h - T_c) \quad , \tag{4}$$

where K_c is the thermal conductance between the housing and cone. K_c is given by

$$K_c = \Sigma \frac{ki\, Ai}{\ell_i} \quad , \tag{5}$$

where k_i = thermal conductivity of connection i

A_i = cross-sectional area of connection i

ℓ_i = length of connection i .

The cone is supported by fiberglass - reinforced epoxy tubes of 1/4 inch O. D. and 3/16 inch I. D., all 2 inches long. The material has a thermal conductivity of 7.46×10^{-3} W/in C. Each support therefore contributes a conductance of $0.801 \times 10^{-4}\, WK^{-1}$. The electrical leads between the housing and cone consist of four, 2×10^{-3} inch diameter nickel (0.76 W/cm C) detector wires and five, 3.145×10^{-3} inch diameter chromel (0.13 W/cm C) temperature measurement and control wires. The wires therefore contribute a conductance of $0.185 \times 10^{-4}\, WK^{-1}$.

The thermal paths through the multilayer insulation between the outside cone areas and the instrument housing may also be treated as conductive. Including the effects of penetration and imperfections, the multilayer has an equivalent thermal conductivity of 1×10^{-6} W/cm C. The outer cone surface area is about 125 in^2. A 1.0 inch thickness of multilayer, therefore, has a thermal conductance of $3.175 \times 10^{-4}\, WK^{-1}$. The total thermal conductance for 8 cone support tubes is then $9.77 \times 10^{-4}\, WK^{-1}$.

For a cone end area A_d of 40.6 in^2, the thermal balance equation of the cone yields

$$4.82 \times 10^{-12} T_c^4 + 3.73 \times 10^{-6} T_c = 5.18 \times 10^{-3} \text{ Wcm}^{-2}$$

for $\beta_s = 15^o$. The solution is

$$T_c = 175.1 \text{ K} .$$

The thermal balance equations for $\beta_s = 12$ degrees and 0 degrees yield

$$T_c = 166.9 \text{ K}, \beta_s = 12^o$$

$$T_c = 166.4 \text{ K}, \beta_s = 0^o .$$

It is seen that the cone temperature is nearly constant for elevation angles of 12 degrees and less.

We will now consider variations in the cone support and ratio of cone end to cone mouth area in order to determine their influence on the cone temperatures. These variations include the limiting cases of a negligible thermal conductance (K_c) and a very large cone end to cone mouth area ratio (A_d/A_m).

First consider changes in the number of cone supports to 6 and 10 tubes. The resultant thermal balance equations at a sun angle of 15 degrees yield

$$4.82 \times 10^{-12} T_c^4 + \begin{Bmatrix} 3.12 \\ 4.34 \end{Bmatrix} \times 10^{-6} = \begin{Bmatrix} 5.00 \\ 5.38 \end{Bmatrix} \times 10^{-3} \text{ Wcm}^{-2} .$$

The solutions are

$$T_c = \begin{Bmatrix} 174.4 \\ 175.9 \end{Bmatrix} \text{ K} .$$

Thus a variation of ± 2 in the number of cone supports produces a variation in cone temperature of less than ± 0.5 percent.

In the limiting case of no conductive coupling between the cone and instrument housing ($K_c \longrightarrow 0$), the cone temperature at the 15 degree sun angle is reduced to 170 K. This is further evidence that the cone temperature is largely determined by the radiative inputs.

Next consider changes in the cone top area ratio to values of 2 and 3. The resultant thermal balance equations at a sun angle of 15 degrees yield

$$4.82 \times 10^{-12} T_c^4 + \begin{Bmatrix} 4.61 \\ 3.07 \end{Bmatrix} \times 10^{-6} T_c = \begin{Bmatrix} 5.53 \\ 4.92 \end{Bmatrix} \times 10^{-3} \text{ Wcm}^{-2} .$$

The solutions are

$$T_c = \begin{Bmatrix} 176.9 \\ 173.7 \end{Bmatrix} \quad K \ .$$

The rate of change of cone temperature with area ratio is greater for a reduction in the ratio than for an increase. In the limit of a very large ratio ($A_d/A_m \longrightarrow \infty$), the cone temperature is reduced to 166.5 K. This limit is equivalent to no conductive input from the housing and no radiative input into the cone mouth.

3.2 Patch Temperature Range

The thermal balance equation for the patch is

$$\sigma A_p T_p^{\,4} = \Phi_K + \Phi_r + \Phi_o + \Phi_j \ , \qquad (6)$$

where A_p = black radiating area of patch

Φ_K = conductive input from cone

Φ_r = radiative input from cone walls above A_p

Φ_o = radiative input through optical openings

Φ_j = joule heating of detectors

The radiative input from the low-emissivity cone walls above the black patch area is given by

$$\Phi_r = \sigma A_p \ \epsilon_{pc} \ T_c^{\,4} \qquad (7)$$

where ϵ_{pc} is the effective patch-to-cone emissivity. For an effective specular cone wall emissivity ϵ_c of 0.05, ϵ_{pc} is 0.04015 and for a wall emissivity of 0.07, 0.0560 (Section 5.0). The resultant radiative inputs for the three sun angles are listed in Table 5. The patch top area A_p is 2.79 in.^{2} when a clearance of 0.05 inch is allowed between the patch and cone wall.

Table 5

Radiative Input from Cone Walls to Patch

		Φ_r for ϵ_c equal to	
β_s	T_c (K)	0.05	0.07
0^o	166.4	3.140×10^{-3} W	4.379×10^{-3} W
12^o	167.1	3.193×10^{-3}	4.453×10^{-3}
15^o	175.1	3.850×10^{-3}	5.369×10^{-3}

The patch is supported by two synthane tubes of 1/8 inch OD, 3/32 ID, and 4 inch length. The electrical leads from the cone to the patch consist of four 2×10^{-3} diameter nickel detector wires and three 3.145×10^{-3} inch diameter chromel temperature measurement and control wires. There is a 1-inch thickness of multilayer insulation between the bottom and sides of the patch and the cone structure. Multilayer at a warm plate temperature equal to that of the cone has an equivalent thermal conductivity of about 0.5×10^{-6} W cm^{-1} K^{-1} in a blanket of 20 layers (NASA SP-5027, Thermal Insulation Systems, P. E. Glaser, et. al., 1967, Figure 37). The bottom and side area of the patch is about 6.8 in^2. The total conductance from the cone to the patch through supports, electrical leads, and insulation is then 3.66×10^{-5} WK^{-1}.

The value of the radiative input through two optical openings to the patch is estimated in Appendix I. The result is

$$\Phi_o \quad 1.8 \times 10^{-3} \text{ W} .$$

The thermal balance equations for the three sun angles then yield for $\Phi_j \quad 0.6 \times 10^{-3}$ W and $\epsilon_c = 0.07$,

$$10.2 \times 10^{-11} T_p^4 + 3.66 \times 10^{-5} T_p \quad \left\{ \begin{matrix} 12.9 \\ 13.0 \\ 14.2 \end{matrix} \right\} \times 10^{-3} \text{ W} ,$$

The solutions are

$$T_p \quad \left\{ \begin{matrix} 97.9 \\ 98.0 \\ 100.8 \end{matrix} \right\} \text{ K} .$$

For $\epsilon_c \quad 0.05$, the thermal balance equations yield

$$10.2 \times 10^{-11} T_p^4 + 3.66 \times 10^{-5} T_p = \left\{ \begin{matrix} 11.6 \\ 11.7 \\ 12.7 \end{matrix} \right\} \times 10^{-3} \text{ W} .$$

The solutions are

$$T_p = \left\{ \begin{matrix} 94.5 \\ 94.8 \\ 97.3 \end{matrix} \right\} \text{ K} .$$

A reduction in the effective cone wall emissivity therefore reduces the patch temperature by 3.2 K to 3.5 K.

We have already considered the influence on the patch temperature of variations in the radiative input from the cone walls (Φ_r). We will now extend this to include variations in the conductive input (Φ_K) and in the fixed (detector) thermal input ($\Phi_o + \Phi_j$).

In the worst case ($\beta_s = 15^o$, $\epsilon_c = 0.07$), an increase in the length of the patch supports to 5 inches and in the thickness of the multilayer insulation to 1.25 inches reduces the patch temperature by 1.3 K. A reduction to 4 inches and 0.75 inch, respectively, increases the patch temperature by 1.8 K. In the limit of no conductive input ($K_c \longrightarrow 0$), T_p becomes 93.5 K.

A reasonable change in the fixed thermal input is 0.6×10^{-3} W. An increase of this amount would result from a doubling of the detector bias heat (to 0.6×10^{-3} W per detector). A change of this amount would result from reasonable variations in the size of the optical opening on the side of the patch. A subtraction of the above amount decreases the patch temperature by 1.4 K, and an addition of the same amount increases the temperature by 1.3 K. In the limit of no fixed thermal input ($\Phi_o + \Phi_j \longrightarrow 0$), T_p becomes 95.0 K ($\beta_s = 15^o$, $\epsilon_c = 0.07$).

3.3 Influence of Solar Panel

A typical mounting of the radiant cooler with respect to the solar panel on the Nimbus spacecraft is shown in Figure 7. The solar panel is shown in the vertical position, where the axis of the cooler is assumed to lie in the plane of the panel. The cooler (shield) mouth is shown at the edge of the instrument mounting surface and 10 inches below it. We will estimate the view factor to the solar panel from the center of the cooler patch under these conditions. The effect of the cone is accounted for by limiting the upward view from the patch to 50 degrees from the cooler axis.

The patch center sees only the 5/16 inch wide bottom of the solar panel in the above position. The view factor is then given by the contour integral of $\sin^2 \vartheta$ about the rectangle shown in Figure 8 (See Section 5.1).

$$\pi F^A_{p\text{-}sp} = \int_0^{\varphi_2} \sin^2 \vartheta_1 \cdot d\varphi + \int_{\varphi_2}^{0} \sin^2 \vartheta_3 \cdot d\varphi \quad , \tag{8}$$

where ϑ and φ are the spherical coordinate angles from the patch center with the cone axis (patch normal) as the pole. Boundary line 2 has an equation of the form φ = constant and therefore does not contribute to the contour integral. The equations for the remaining two boundary lines are of the form given by Equation 22 and the integrals of the form given by Equation 24 (Section 5.1).

For the geometry of Figure 8, we have

$$\cos \beta_1 = 0.7660$$

$$\cos \beta_3 = 0.6192$$

$$\tan \varphi_2 = 0.00470$$

and $$F^A_{p\text{-}sp} = 9.6 \times 10^{-4} .$$

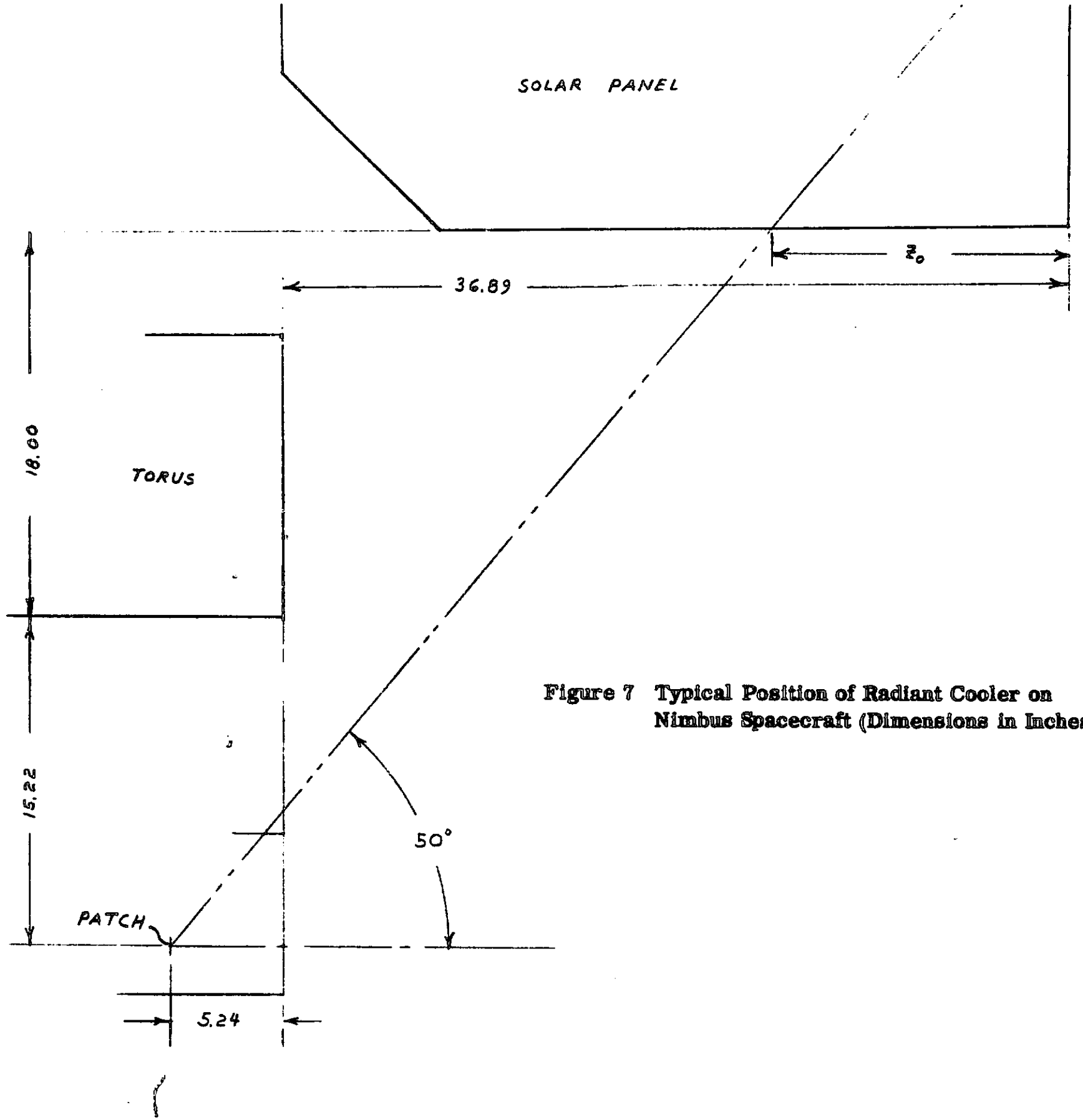

Figure 7 Typical Position of Radiant Cooler on Nimbus Spacecraft (Dimensions in Inches)

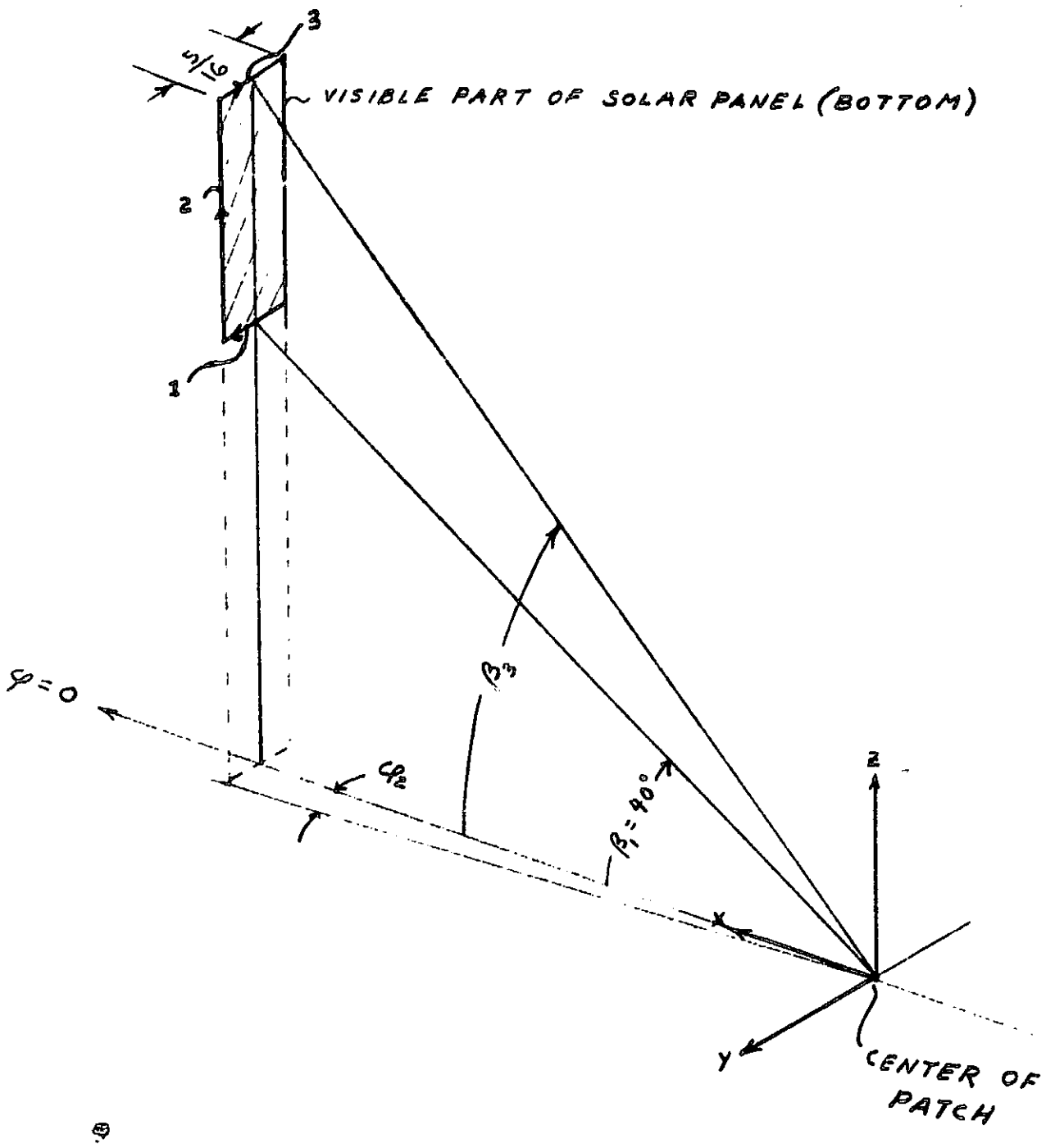

Figure 8 View from Center of Patch to Vertical Solar Panel

If the above view factor is the maximum encountered during the rotation of the solar panel, it can be used to estimate the average view factor over an orbit. The panel is pivoted around an axis 48 inches above and parallel to its bottom surface. When the panel is rotated 49.8 degrees from its vertical position it is no longer visible from the patch because of the 50 degree limit on the upward view. The average view factor from the patch to the solar panel is then approximately 1/2 x 49.8/90 of its maximum value, or

$$\text{av. } F_{p\text{-}sp} \cdot 2.6 \times 10^{-4} .$$

To test the above assumption, the view factor was estimated for the solar panel rotated to the position where the bottom length seen from the patch (Z_0 in Figure 7) is one-half its vertical value (about 23.7 degrees from the vertical). For the above estimate of the average view factor to be valid, the view factor in this position should be about one-half the assumed maximum value. In the new position, the area seen from the patch is no longer on the bottom. Instead, the patch sees a triangular region on the side, as shown in Figure 9. Contour integration (Section 5.1) yields

$$2\pi \; F^{B}_{p\text{-}sp} \quad \int 1 + \int 3 \; , \tag{9}$$

where $\int 1 = \cos \alpha_1 \; [\arctan (\cos \alpha_1 \cdot \tan \varphi)]_{\varphi_1}^{\varphi_2}$

$\int 3 \quad \cos \beta_3 \; [\arctan (\tan \varphi / \cos \beta_3)]_{\varphi_2}^{\varphi_1}$.

The middle boundary line again has an equation of the form φ = constant. For the geometry of Figure 9,

$$\cos \alpha_1 = 0.7660$$

$$\cos \beta_3 = 0.39875$$

$$\tan \varphi_1 = 0.3648$$

$$\tan \varphi_2 = 0.4391 .$$

The view factor for this position of the solar panel is then approximately

$$F^{B}_{p\text{-}sp} = 4.8 \times 10^{-4}$$

or one-half the value for a vertical panel, as assumed.

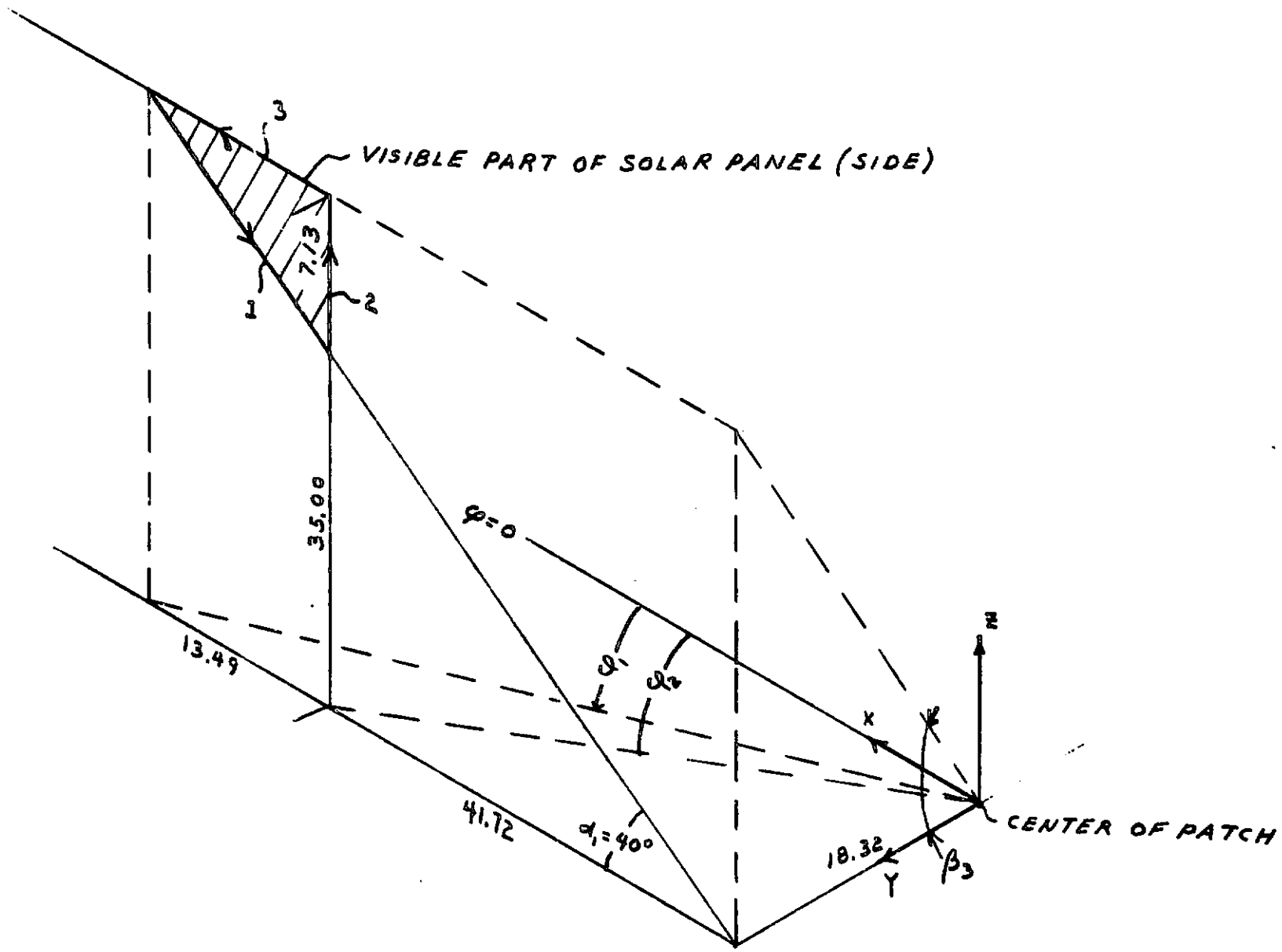

Figure 9 View from Center of Patch to Rotated Solar Panel

If the solar panel is a blackbody at a temperature T_{sp}, it produces an average thermal load on the patch given by

$$\Phi_{sp} = \text{av. } F_{p\text{-}sp}\ A_p\ \sigma T_{sp}^{4}\ , \tag{10}$$

where A_p is the top area of the patch. Because of its relatively long thermal response time, the patch responds to the average thermal input. For $A_p = 2.79\ \text{in}^2$, $T_{sp} = 300\ \text{K}$, and av. $F_{p\text{-}sp} = 2.6 \times 10^{-4}$, we obtain

$$\Phi_{sp} = 0.29 \times 10^{-3}\ \text{W}\ .$$

This produces a temperature rise in the patch (Section 3.2) of about 0.6 K.

4.0 VARIATIONS IN DESIGN

Variations in the design of the radiant cooler were made in the attempt to improve the performance above that of design II. To begin with, consider the use of design III (Section 2.2). The maximum possible improvement of design III over design II (there, in fact, may be no improvement or a degradation) is obtained by assuming that ϵ_{pc} and T_c are unchanged from design II. In addition, we will assume that the thermal conductance between the patch and cone (K_p) is unchanged, i.e., that the larger patch is supported by the same two synthane support tubes, and that the multilayer insulation thickness is increased in proportion to the increased area of the patch sides and bottom. In this case, only the patch radiating area (A_p) increases. The relative increase is

$$\frac{Ap\ III}{Ap\ II} \qquad 1.277 \quad .$$

The thermal balance equation (Section 3.2) for the larger patch area when β_s = 15 degrees, ϵ_c = 0.07, and T_c = 175.1 K then yields

$$10.2 \times 10^{-11}\ T_p^{\ 4} + 2.87 \times 10^{-5}\ T_p \qquad 12.3 \times 10^{-3}\ W \quad .$$

The solution is

$$T_p = 98.2\ K \quad .$$

This is a reduction of 2.6 kelvins.

Rather than analyze design III in detail, design II was modified to obtain an actual reduction in patch temperature (at least) equal to the above limiting value for design III. The cone and patch were unchanged. Instead, a study was made of ways in which to reduce the cone temperature. The cone temperature is largely determined by the radiative inputs to the cone top (Section 3.1). And only about 10 percent of this input is absorbed in the cone mouth. Moreover, most of the radiative input to the low α/ϵ cone end is from the earth. As a result, a significant reduction in the cone temperature requires a significant reduction in the earth radiation absorbed in the cone end.

First, a reduction in the cone end area was traded for a reduction in the view factor from the cone end to the earth. The cone end subarea b (Figure 3) was eliminated. This reduced the view factor, F_{de}, to 0.0828 or by x 0.86. It also reduced the cone end to cone mouth area ratio, A_d/A_m, by 2.05 or by x 0.83. The result is a reduction in the cone temperature by 1 K. If subarea a and b are both eliminated, the reduction becomes 1.5 K. The corresponding reductions in the patch temperature are 0.6 K and 0.9 K, appreciably less than the goal of 2.6 K.

This approach was therefore abandoned, and the view factor to earth was decreased (shading of the cone end increased) without reducing the cone end area. This could be done by tilting subareas a and b away from the earth. Instead, the lower (earthward) shield was extended by 2 inches in the direction parallel to the cone axis. At the same time the shield was maintained at a 15 degree angle to the cone axis and moved 0.527 inch in the nadir direction so that it was still not visible from the patch. The maximum linear dimension was maintained at 12 inches. The top view is shown in Figure 10. The remainder of the cooler design is identical to design II. In addition to increasing the shading of the cone top, this modification also reduces the influence of radiative inputs to the cone mouth and conductive inputs from the housing by increasing the cone end area.

The following parameters were calculated for modified design II using the techniques developed and applied to design II in Sections 5.0 and 6.0.

$$F_{d-e} = 0.0615$$

$$\alpha_{me} = 2.29 \times 10^{-2}$$

$$\epsilon_{me} = 5.80 \times 10^{-3}$$

$$\alpha_{ms} = 1.7 \times 10^{-3}$$

$$a_{dh} = 1.904 \times 10^{-2}$$

$$g_d = \begin{cases} 0, & \beta_s = 0^o \\ 0.0107, & \beta_s = 12^o \\ 0.101, & \beta_s = 15^o \end{cases} .$$

For $A_m/A_d = 1/2.81$, $\epsilon_d = 0.85$, $\alpha_d = 0.25$, $A_d = 46.2\ in^2$, $T_h = 308\ K$, and $K_c = 9.77 \times 10^{-4}\ WK^{-1}$, the thermal balance equation of the cone (Section 3.1) yields for the three sun angles

$$4.82 \times 10^{-12}\ T_c^4 + 3.28 \times 10^{-6}\ T_c = \begin{Bmatrix} 3.37 \\ 3.44 \\ 4.29 \end{Bmatrix} \times 10^{-3}\ Wcm^{-2} .$$

The solutions are

$$T_c = \begin{Bmatrix} 156.0 \\ 157.0 \\ 167.0 \end{Bmatrix} K .$$

The respective reductions in cone temperature compared with design II are 10.4 K, 9.9 K, and 8.1 K. The relative decrease in the thermal input from the earth is shown in Table 6, which lists each thermal load on the cone as a percentage of the total.

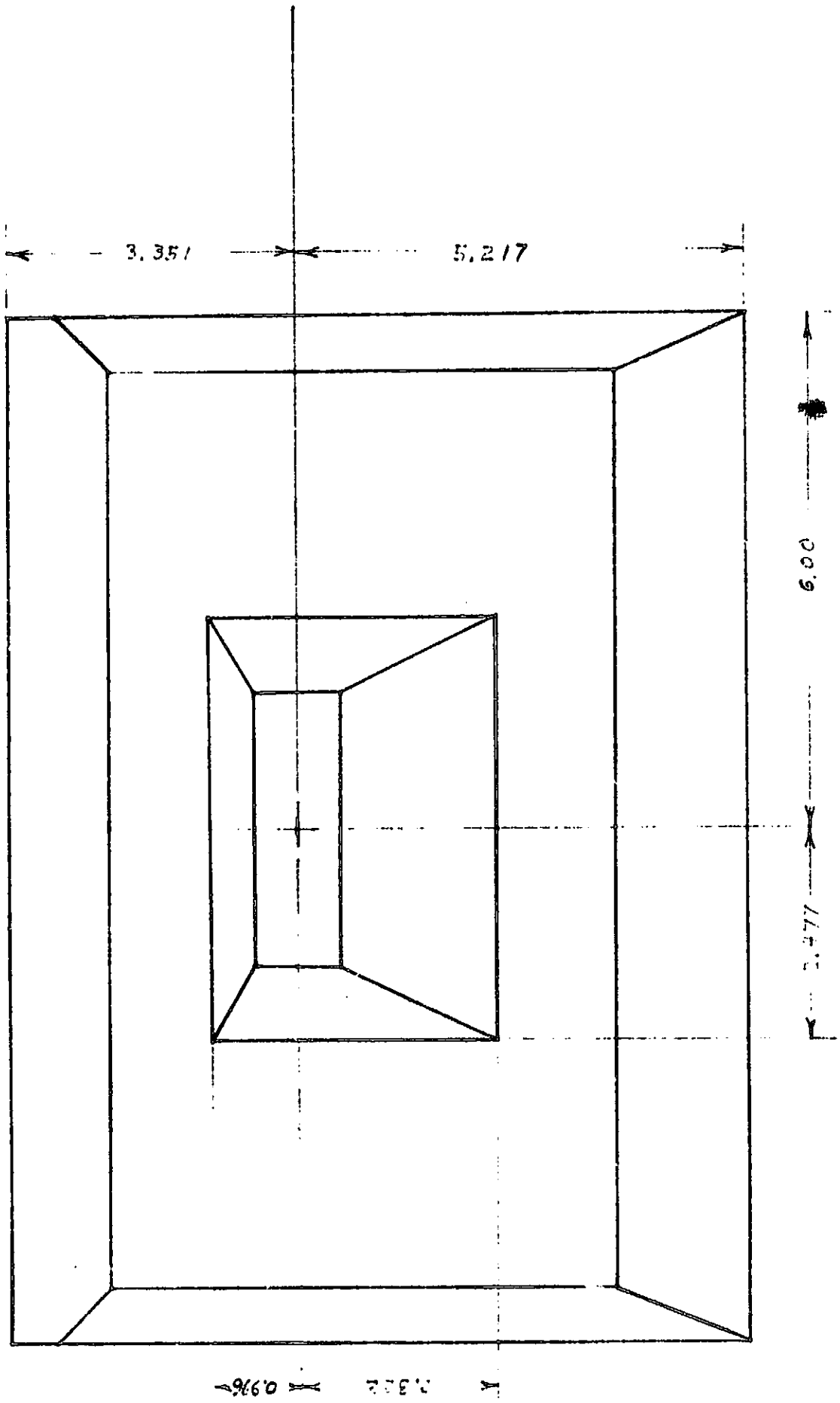

Figure 10 Top View of Modified Design II

Table 6

Distribution of Thermal Inputs to Cone

β_s	Earth	Shield	Direct Solar	Conductive
		Design II		
0^o	71.8%	16.8%	0%	11.4%
12^o	70.2	16.5	1.4	11.9
15^o	59.0	13.9	17.0	10.1
		Modified Design II		
0^o	53.7	28.9	0	17.4
12^o	52.2	28.2	2.7	16.9
15^o	40.6	22.1	25.0	12.3

The cone and patch are unchanged from design II, so that the equations and data of Section 3.2 can be used to calculate the patch temperature range for the above cone temperature range. The results are listed in Table 7. It is seen that the modification meets the goal of a temper ature reduction of 2.6 K or more for all combinations of cone wall emissivity and sun angles except one. Moreover, the patch temperature is safely below the upper limit of 100 K in all cases.

Table 7

Patch Temperature Range of Modified Design II

		T_p		$-\Delta T_p$	
β_s	$\epsilon_c \rightarrow$ 0.07		0.05	0.07	0.05
0^o	94.3 K		91.6 K	3.6 K	2.9 K
12^o	94.5		91.9	3.4	2.9
15^o	98.0		94.8	2.8	2.4

The distribution of thermal inputs to the patch at a cone wall emissivity of 0.05 is given in Table 8 for the three sun angles. Note that it is approximately balanced among the radiative, conductive, and detector sources.

Table 8

Distribution of Thermal Inputs to Patch

$\epsilon_c = 0.05$

β_s	Radiative (Φ_r)	Conductive (Φ_K)	Detector ($\Phi_o + \Phi_j$)
0^o	33.8%	32.8%	33.4%
12^o	34.2	32.9	32.9
15^o	38.7	32.2	29.1

5.0 VIEW FACTORS

In order to determine the radiative interchange between two radiant cooler areas and between a cooler area and an external area, it is necessary to know one or several view factors (The fraction of power diffusely emitted from one area that directly strikes a second area is the view factor from the first area to the second). The view factors required for thermal analysis of the radiant cooler are:

(a) $F_{p-m\ (n)}$ = view factor from the patch to the cone mouth images seen by n specular reflections in the cone walls,

(b) $F_{d-h\ (n)}$ = view factor from the cone end to the shield mouth images seen by n specular reflections in the shield wall,

(c) F_{d-e} = view factor from the cone end to the visible region of the earth,

(d) $F_{m-e\ (n)}$ = view factor from the cone mouth to the visible region of the earth whose radiation is reflected n times in the cone walls.

The view factors (a) are used to determine the patch-cone radiative coupling factor or effective patch-to-cone emissivity. (Final Report on Contract NAS5-10113, December 1967, Section 1.3),

$$\epsilon_{pc} = 1 - \sum_n F_{p-m\ (n)}\ (1 - \epsilon_c)^n, \tag{11}$$

where ϵ_c is the emissivity of the cone walls and the patch is black (emissivity of one).

The view factors(b) are used to determine the effective emissivity of the shield as seen from the cone end (equal to the effective absorptivity of the shield for cone end radiation),

$$a_{dh} = \sum_n a_n\ F_{d-h\ (n)}, \tag{12}$$

where a_n is the emissivity (absorptivity) produced by n shield wall reflections. For infrared radiation, $a_n = 1 - (1 - \epsilon_h)^n$, where ϵ_h is the infrared absorptivity (emissivity) of the shield walls. Using the conservation condition

$$\Sigma F_{d-h\ (n)} = 1, \tag{13}$$

the above may also be written as

$$a_{dh} = 1 - \Sigma F_{d-h\ (n)}\ (1 - \epsilon_h)^n. \tag{14}$$

The cone end shield radiative coupling factor or effective emissivity is obtained by multiplying a_{dh} by the emissivity ϵ_d of the cone end. This is the case because radiation leaving the cone end by emission or reflection never returns when the shield

walls are specularly reflecting and outward sloping (a condition which also holds between the patch and cone walls).

The view factors (c) and (d) are used to determine the absorptivity of the cone end and cone mouth, respectively, for radiation from the earth. In the case of the cone mouth, multiple reflections at the cone walls must be taken into accout. The effective absorptivity for earth radiation is then

$$a_{me} = \Sigma a_n \; F_{m-e\,(n)}\,, \tag{15}$$

where a_n is the absorptivity produced by n cone wall reflections. For infrared from the earth, $a_n = 1 - (1 - \epsilon_c)^n$ and for reflected sunlight, $a_n = 1 - (1 - \alpha_c)^n$, where ϵ_c and α_c are the infrared absorptivity (emissivity) and solar absorptivity, respectively.

5.1 Basic Equations

In general, there are two types of view factors, those from an area to a region bounded by straight lines (view factors a and b) and those from an area to the earth or a subregion of the earth (view factors c and d). As an example of the first type, consider the view factor $F_{p-m(n)}$ from the patch to the cone mouth as seen by n specular reflections in the cone walls. The patch is divided into elemental areas from which the view factors $F_{j-m(n)}$ are calculated. The view factor from the entire patch is then (M. Jakob, Heat Transfer, Vol. II, Wiley 1957, Section 31-6)

$$F_{p-m(n)} = \frac{1}{A_p} \sum_j F_{j-m(n)} * A_j\,, \tag{16}$$

where A_p is the patch area viewing the cone walls (top of the patch) and A_j the area of a patch element.

Each elemental view factor is given by

$$F_{j-m(n)} = \frac{1}{\pi} \iint_{m(n)} \cos\vartheta \cdot \sin\vartheta \cdot d\vartheta \cdot d\varphi, \tag{17}$$

where ϑ and φ are the spherical coordinates with respect to a normal to the patch element and the integration is over the angles subtended by the cone mouth as seen by n specular cone wall reflections. Integrating with respect to ϑ, this becomes a contour integral about the boundaries of the n cone mouth images,

$$F_{j-m(n)} = \frac{1}{2\pi} \oint_{m(n)} \sin^2\vartheta\,(\varphi) \cdot d\varphi. \tag{18}$$

The problem of determining the radiative coupling factor between the patch and cone has thus been reduced to that of the calculating contour integrals about the boundary of the cone mouth and its images. And in the case of a radiant cooler of rectangular geometry (such as that considered here), the boundaries are composed of line segments.

For zero cone wall reflections, the integration is around the boundary of the cone mouth itself, so that we have

$$2\pi\ F_{j-m(o)} = \sum_{j=1}^{4} \int_{\varphi ij}^{\varphi jk} \sin^2\ \vartheta j\ (\varphi)\ .\ d\ \varphi, \qquad (19)$$

where φij and φjk are the azimuth angles of the intersection of the boundary line j with boundary lines i and k. A straight line in spherical coordinates has an equation of the general form

$$\sin^2 \vartheta_{\ell} = \left[1 + \cos^2 (\varphi + \varphi_o) (\tan \beta - \tan \alpha .\ \tan <\varphi + \varphi_o>)^2\right]^{-1}, \qquad (20)$$

where the angles φ_o, β, and α are shown in Figure 11. The integration of the $\sin^2 \vartheta_{\ell}$ is carried out by setting $\varphi' = \varphi + \varphi_o$ and using the result

$$\int \frac{d\varphi'}{1 + \cos^2 \varphi' (\tan \beta - \tan \alpha \cdot \tan \varphi', ^2} = \frac{2}{\sqrt{4ac - b^2}}\ \text{arctg}\left[\frac{2a \tan \varphi' + b}{\sqrt{4ac - b^2}}\right], \qquad (21)$$

where

$a = 1 + \tan^2 \alpha,$

$b = -2 \tan \alpha \cdot \tan \beta,$

$c = 1 + \tan^2 \beta.$

For the simpler case of an untilted cooler (i.e., of the patch in a vertical plane), the angle α for n equal to zero is also zero. If the $\varphi = 0, \pi$ plane is either the vertical or the horizontal plane (i.e., either of the usual sections of an untilted cone), the boundary lines perpendicular to the plane have equations of the form

$$\sin^2 \vartheta_i = (1 + \cos^2 \varphi .\ \tan^2 \beta_i)^{-1}, \qquad (22)$$

where β_i is the elevation angle of the line above the surface of the patch in the $\varphi = 0, \pi$ plane. The boundary lines perpendicular to the $\varphi = \pi/2,\ 3\pi/2$ plane have equations of the form,

$$\sin^2 \vartheta_j = (1 + \sin^2\ \varphi \cdot \tan^2 \beta j)^{-1}, \qquad (23)$$

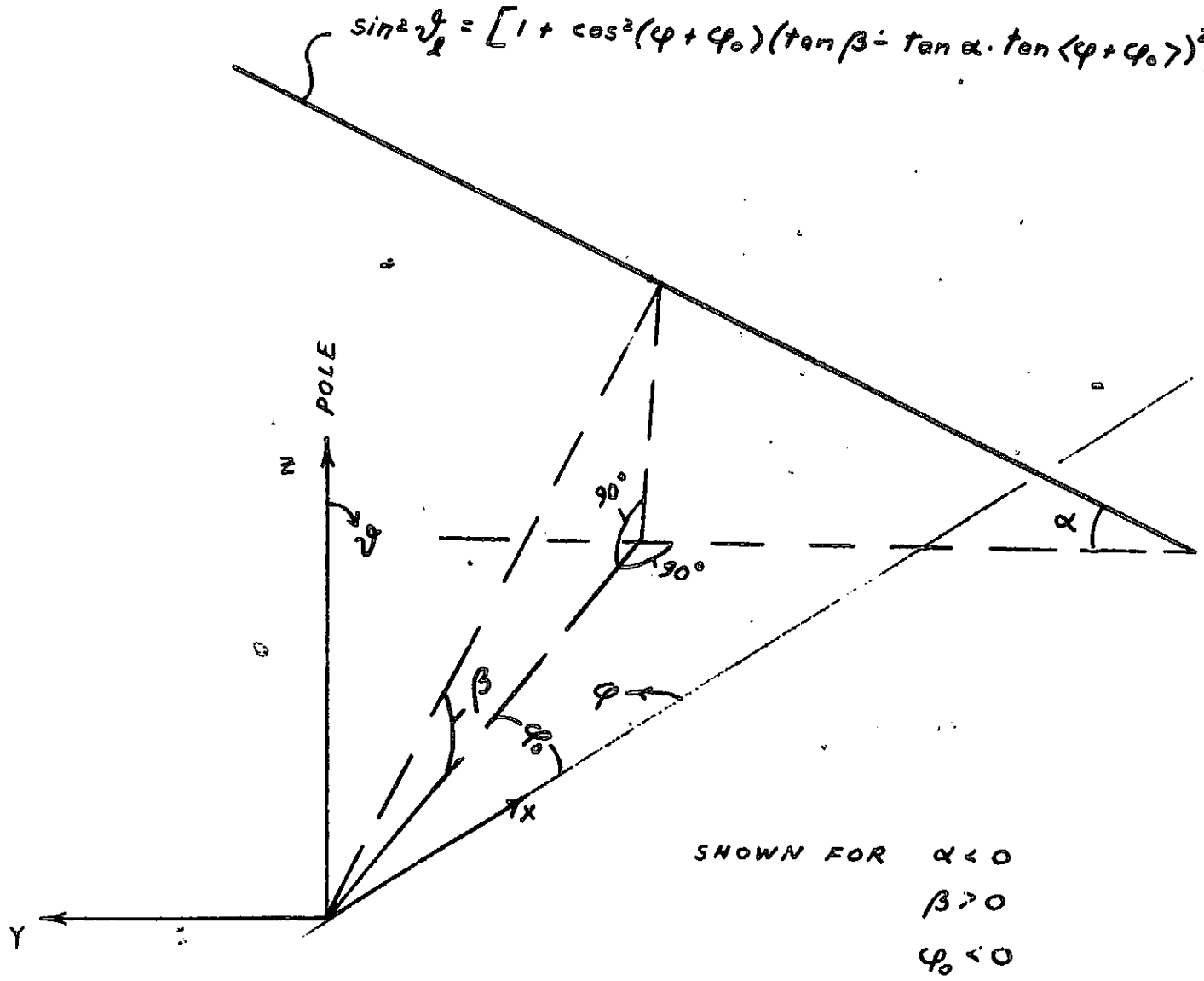

Figure 11 Straight Line in Spherical Coordinates

where βj is the line elevation angle in the $\varphi = \pi/2,\ 3\pi/2$ plane. The azimuth angle of the intersection of two boundary lines is obtained by setting $\vartheta_i = \vartheta_j$. Integration then yields

$$\int \sin^2 \vartheta_i \cdot d\varphi = \cos \beta_i \cdot \arctan (\tan \varphi \cdot \cos \beta_i), \tag{24}$$

$$\int \sin^2 \vartheta_j \cdot d\varphi = \cos \beta_j \cdot \operatorname{actan} (\tan \varphi / \cos \beta_j). \tag{25}$$

Only part of the cone mouth image may be visible from the patch for n equal to 1 or more. The limit is set by the plane of the top of the patch itself ($\sin^2 \vartheta = 1$). The intersection of the cone mouth image with the plane of the patch then forms one of the boundaries of the contour integration.

The radiative coupling factor between the cone end and any earth/sun shield is of the same form as that for the patch-cone interchange. In addition to other cooler areas, however, the cone walls and cone end can see external areas. These may include spacecraft structure and adjacent instruments as well as the sun and earth. Because the sun produces an essentially collimated (narrow angle) beam at the earth, it is not necessary to consider the view factor to the sun, but only its direction with respect to the area of interest (see section 7.0). On the other hand, the earth subtends a wide range of angles from a spacecraft in near-earth orbit.

The dimensions of the cooler are negligible compared with those of the earth, so that the equation for the earth's horizon from a cooler surface does not depend on its location but only on its orientation (i.e., the direction of its normal with respect to the earth). The equation for the earth's horizon as seen from a vertical cooler surface is

$$\sin^2 \vartheta_e = \sec^2 \varphi \cdot \cos^2 \beta_e, \tag{26}$$

where β_e is the angle from the spacecraft nadir to a tangent line to the earth's surface from the spacecraft. Integration over a boundary formed by the earth's horizon then yields

$$\int \sin^2 \vartheta_e \cdot d\varphi = \tan \varphi \cdot \cos^2 \beta_e. \tag{27}$$

The remaining boundary of the visible earth is formed either by boundaries within the cooler or by the plane of the vertical surface itself ($\sin^2 \vartheta = 1$). The view factor from a vertical surface for which there is no shielding of the earth is given by

$$F_{ve} = \frac{1}{2\pi} \int_{-\beta_e}^{\beta_e} 1 \cdot d\varphi + \frac{1}{2\pi} \int_{\beta_e}^{-\beta_e} \sin^2 \vartheta_e \cdot d\varphi,$$

where β_e is also the azimuth angle of the intersection of the earth's horizon with the vertical surface ($\sec^2 \varphi \cdot \cos^2 \beta_e = 1$). We then obtain

$$F_{ve} = \frac{1}{\pi} (\beta_e - \sin \beta_e \cdot \cos \beta_e). \tag{28}$$

However, not all cooler surfaces are vertical. The upper and lower cone walls are tilted out of a vertical plane as are many of the images of the cone walls formed by specular reflections within the cone. The view factor to earth from a tilted surface in the absence of shielding is given by Hottel and Sarofim (Radiative Transfer, McGraw-Hill, 1967, Section 2.10),

$$F_{te} = \frac{1}{\pi} \left[\cos^{-1} \left(\frac{\cos \beta_e}{\cos \alpha} \right) - \sin \beta_e \cdot \cos \beta_e \cdot \cos \alpha \cdot \left(1 - \frac{\tan^2 \alpha}{\tan^2 \beta_e} \right)^{1/2} - \sin^2 \beta_e \cdot \sin \alpha \cdot \cos^{-1} \left(\frac{\tan \alpha}{\tan \beta_e} \right) \right], \tag{29}$$

where the surface normal is tilted an angle α above the horizontal.

When there is shielding of the earth for a tilted surface, it is necessary to know the equation for the earth's horizon as seen from the tilted surface,

$$\sin^2 \vartheta_e (\varphi) \cdot d\varphi = \sin^2 \beta_e (\cos \alpha \cot \beta_e \cos \psi + \sin \alpha)\, d\psi, \tag{30}$$

where

$$\tan \varphi = \frac{\sin \psi}{\cos \alpha \cot \beta_e + \sin \alpha \cos \psi}, \tag{31}$$

Integration yields

$$\int \sin^2 \vartheta_e \cdot d\varphi = \sin^2 \beta_e (\cos \alpha \cot \beta_e \sin \psi + \psi \sin \alpha). \tag{32}$$

These results are derived in Appendix II. They can also be obtained from the results of Hottel and Sarofim (Radiative Transfer, McGraw-Hill, 1967, Section 2.10) and the equation relating φ (azimuth angle in the plane of the tilted cooler surface) and ψ (azimuth angle in the plane of the earth equivalent circular disk). The symmetry condition (equal views to earth on either side of the y-z plane) imposed by Hottel and Sarofim is not a necessary condition for the result to hold as long as the normal to the tilted surface lies in the y-z plane (and the coordinate system can always be set up to meet this condition).

The array of cone mouth images (or cone walls and their images) formed by specular reflection in the cone walls view the earth through the cone walls and the cone mouth. Each, therefore, absorbs earth radiation in proportion to its view factor

to the earth. This approach, however, was found to be very complex and quite unsatisfactory. Not only was the geometry complicated by the tilted surfaces, but also by the many boundaries between the image and the earth that may limit its view to earth.

We therefore changed to the view of earth from the cone mouth itself. The view factor to earth, F_{me}, can be calculated for any element on the cone mouth. This view factor, in turn, is divided into view factors inward from the cone mouth element to images (in general, partial images) of the cone mouth formed by reflection in the cone walls. The view factor to the (partial) nth cone mouth images is equal to that part of F_{me} in which rays are reflected n times before going to earth by way of the cone mouth element. Or, viewed another way, the images of the cone mouth may be projected through the cone mouth element onto that portion of the earth visible from the element (See Figure 12). This divides the earth into regions whose radiation undergoes known numbers of reflections at the cone walls before going back out the cone mouth. The problem of determining the cone wall absorptivity for earth radiation is then reduced to that of determining view factors from an untilted surface to regions bounded by the earth's horizon and by straight lines.

5.2 View Factors for Radiant Cooler Design II

For purposes of calculating the view factors(a), the patch was divided into 16 equal elements. By symmetry, there are 8 different view factors (from elements A through H in Figure 3). Since the elements are equal in size, the view factor from the entire patch is just the average elemental view factor. It is shown in Appendix III that the view factor from the patch to the cone mouth images formed by 3 reflections is negligible. It is therefore necessary to calculate only $F_{p-m\ (0)}$ and $F_{p-m\ (1)}$ and determine $F_{p-m\ (2)}$ from the conservation equation

$$\Sigma F_{p-m\ (n)} = 1.$$

The results are listed in Table 9.

TABLE 9

View Factors from Patch to Cone Mouth Images

Element	Fp-m (o)	Fp-m (1)	Fp-m (2)
A	0.3289	0.50845	0.16265
B	0.3527	0.4977	0.1496
C	0.3686	0.48085	0.14055
D	0.3765	0.5020	0.1215
E	0.3044	0.5158	0.1798
F	0.3263	0.5048	0.1689
G	0.3409	0.5012	0.1579

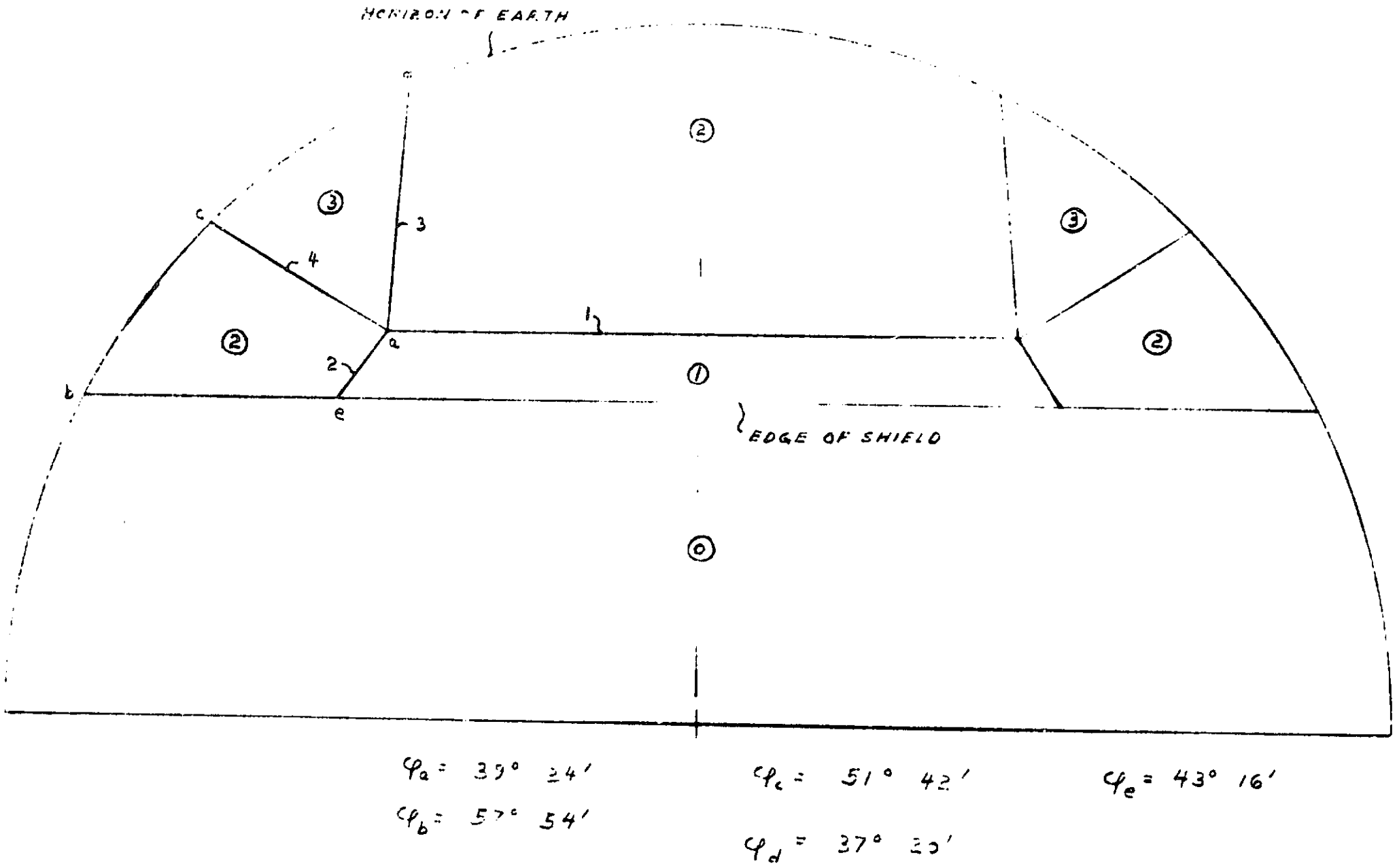

Figure 12 Equivalent Earth for Cone Wal: Absorption as Seen from Cone Mouth Center (Design II)

TABLE 9 (Cont.)

View Factors from Patch to Cone Mouth Images

Element	Fp-m (0)	Fp-m (1)	Fp-m (2)
H	0.3482	0.4998	0.1520
Patch	0.3433	0.5026	0.1541

The above view factors were also estimated by their values from the center of the patch. The results are listed in Table 10. Use of this approximation greatly simplifies the calculation of the patch-cone radiative coupling factor. For a given cone wall emissivity in design II, use of values of Fp-m (n) from the center of the patch in place of the average from the eight patch elements results in an error (reduction) in the radiative coupling factor of 5.3%. The resultant error in the calculated patch temperature is then less than one-fourth this amount.

TABLE 10

View Factors from Patch Center to Cone Mouth Images:

n	Fp-m (n)
o	0.3656
1	0.5019
2	0.1325

The view factors (b) and (c) were calculated from 10 cone end elements. By symmetry, there are five different view factors (from elements a through e in Figure 3). Since the elements are not equal in size, the view factor from the entire cone end is the area-weighted average of the elemental view factors. The results for radiant cooler design II are listed in Tables 11 and 12. Because the view factor to the shield mouth as seen by two shield wall reflections is small, it was taken only from element c, which has view factors close to those of the entire cone end.

TABLE 11

View Factors from Cone End to Shield

Mouth and its Images

Element (i)	F^{i}_{d-h} (0)	Weight (Relative Area)
a	0.6694	0.1946
b	0.7547	0.1678

TABLE 11 (Cont.)

View Factors from Cone End to Shield

Mouth and its Images

Element (i)	$F^{i}_{d-h\,(0)}$	Weight (Relative Area
c	0.7014	0.4689
d	0.5526	0.0906
e	0.6218	0.0781

$$F_{d-h\,(0)} = 0.6844$$

$$F_{d-h\,(1)} = 0.2925$$

$$F_{d-h\,(2)} = 0.0231$$

TABLE 12

View Factors from Cone End to Earth

Element (i)	F^{i}_{d-e}
a	0.1393
b	0.1577
c	0.0908
d	0
e	0
cone end	0.0961

The view factors (d) were calculated from an element at the center of the cone mouth. The projections of the cone mouth images and the shield onto the earth as seen from this element are shown in Figure 12. The region of the earth below the edge of the shield cannot be seen from the cone mouth. The rest of the earth is divided into regions whose radiation is reflected from 1 to 3 times in the cone walls after passing through the center of the cone mouth. The earth is shown as its equivalent flat disk (See H. C. Hottel and A. F. Sarofim, Radiative Transfer, McGraw-Hill, 1967, Section 2.10). The results of the view factor calculations are listed in Table 13. It is seen that about 69 percent of the earth rays entering the cone mouth undergo two cone wall reflections.

TABLE 13

View Factors from Cone Mouth to Regions

of Visible Earth

n		$F_{m-e\ (n)}$	$F_{m-e\ (n)} / F_{m-e}$
1		0.0217	0.221
2		0.0675	0.688
3		0.0089	0.091
F_{me}	=	0.0981	1.000

6.0 DIRECT SUNLIGHT EXPOSURE

The influence of direct sunlight on the cone of design II was analyzed at solar elevation angles (above the plane of the cone top) of 12 degrees and 15 degrees. At the lower angle, only the cone end is irradiated by direct sunlight while at the higher angle the corners of the cone mouth are also exposed during portions of the orbit. This is shown in Figure 13. The tracks of two of the shield corners projected onto the cone top by the solar rays are shown for sun elevation angles of 12 degrees and 15 degrees. The form of the shadow cast by the shield is indicated at solar azimuth angles (in the plane of the cone top) of 60 degrees and 120 degrees. By symmetry, the exposure pattern for azimuth angles from 360 degrees to 180 degrees is the same as that from 0 degrees to 180 degrees.

Because of the large thermal time constant of the cone structure, the influence of direct sunlight is averaged over an orbital period. The average fraction of cone end area exposed over an orbit (the solar exposure factor) is given by

$$g_d = 1/\pi \int_0^{\pi} g_d(\varphi_s) \cdot d\varphi_s, \tag{33}$$

where $g_d(\varphi_s)$ is the solar exposure factor (fraction of exposed area) at a solar azimuth angle φ_s. The variations of $g_d(\varphi_s)$ with φ_s are given in Figure 14 for solar elevation angles (β_s) of 12 degrees and 15 degrees. There is no need to consider shading by the earth during a portion of the nighttime part of the orbit because g_d is already zero during this period as a result of shading by the cone shield. Integration of the curves in Figure 14 yields

$$g_d(\beta_s = 12^o) = 0.0086$$

$$g_d(\beta_s = 15^o) = 0.0961 .$$

The cone mouth solar absorptivity at a solar azimuth angle φ_s is given by

$$\alpha_{ms}(\varphi_s) = \sum_n \alpha_n \cdot g_n(\varphi_s) , \tag{34}$$

where $\alpha_n = 1 - (1 - \alpha_c)$

α_c = solar absorptivity of cone wall,

$g_n(\varphi_s)$ = fraction of cone mouth area over which direct solar rays incident at φ_s require n reflections to leave the cone.

And the effective solar absorptivity averaged over an orbit is given by

$$\alpha_{ms} = 1/\pi \int_0^{\pi} \alpha_m(\varphi_s) \cdot d\varphi_s = \sum_n \alpha_n \cdot 1/\pi \int_0^{\pi} g_n(\varphi_s) \cdot d\varphi_s,$$

$$\alpha_{ms} = \sum_n \alpha_n \cdot g_n \tag{35}$$

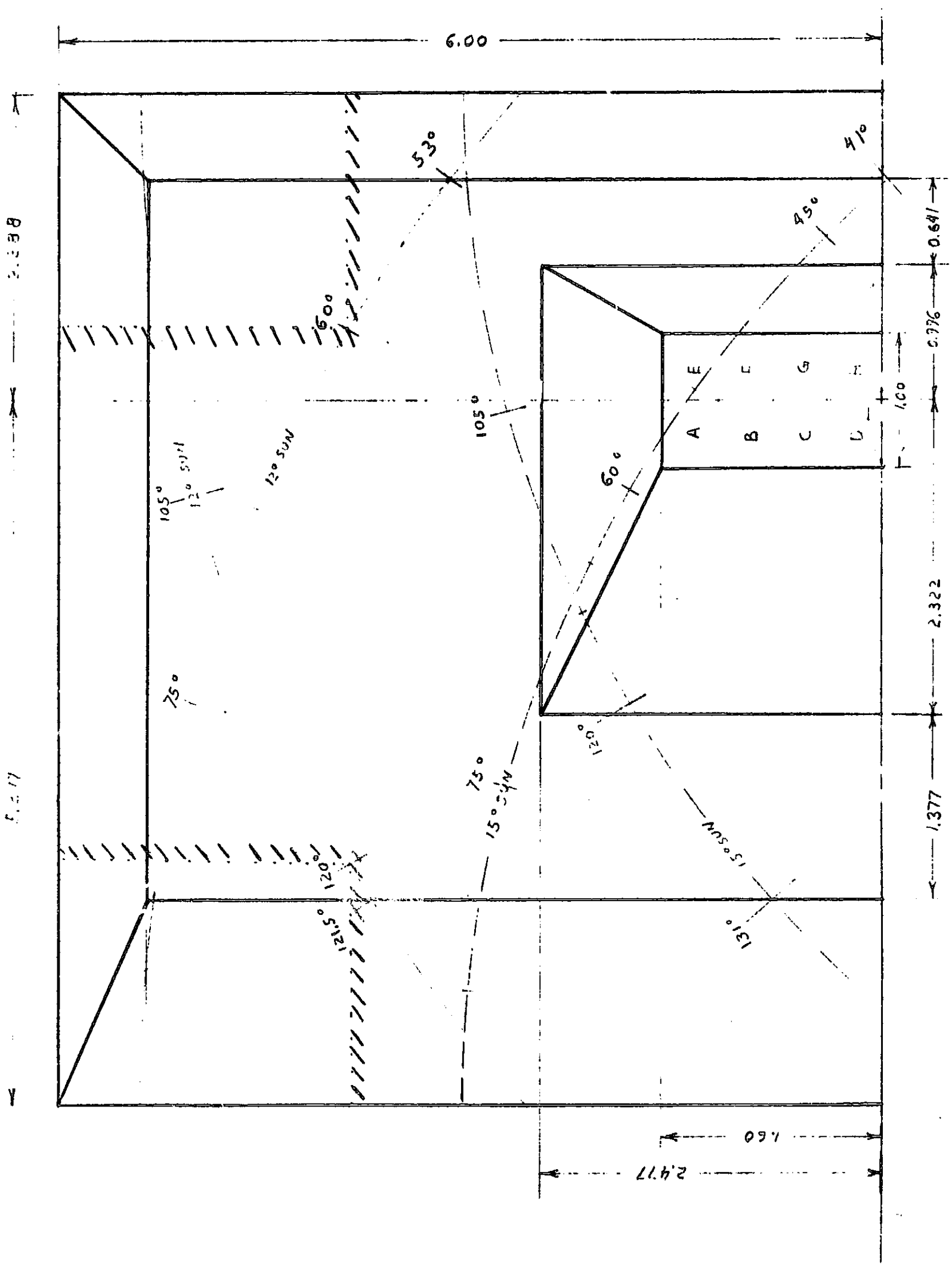

Figure 13 Direct Sunlight Exposure of Cone End (Design II)

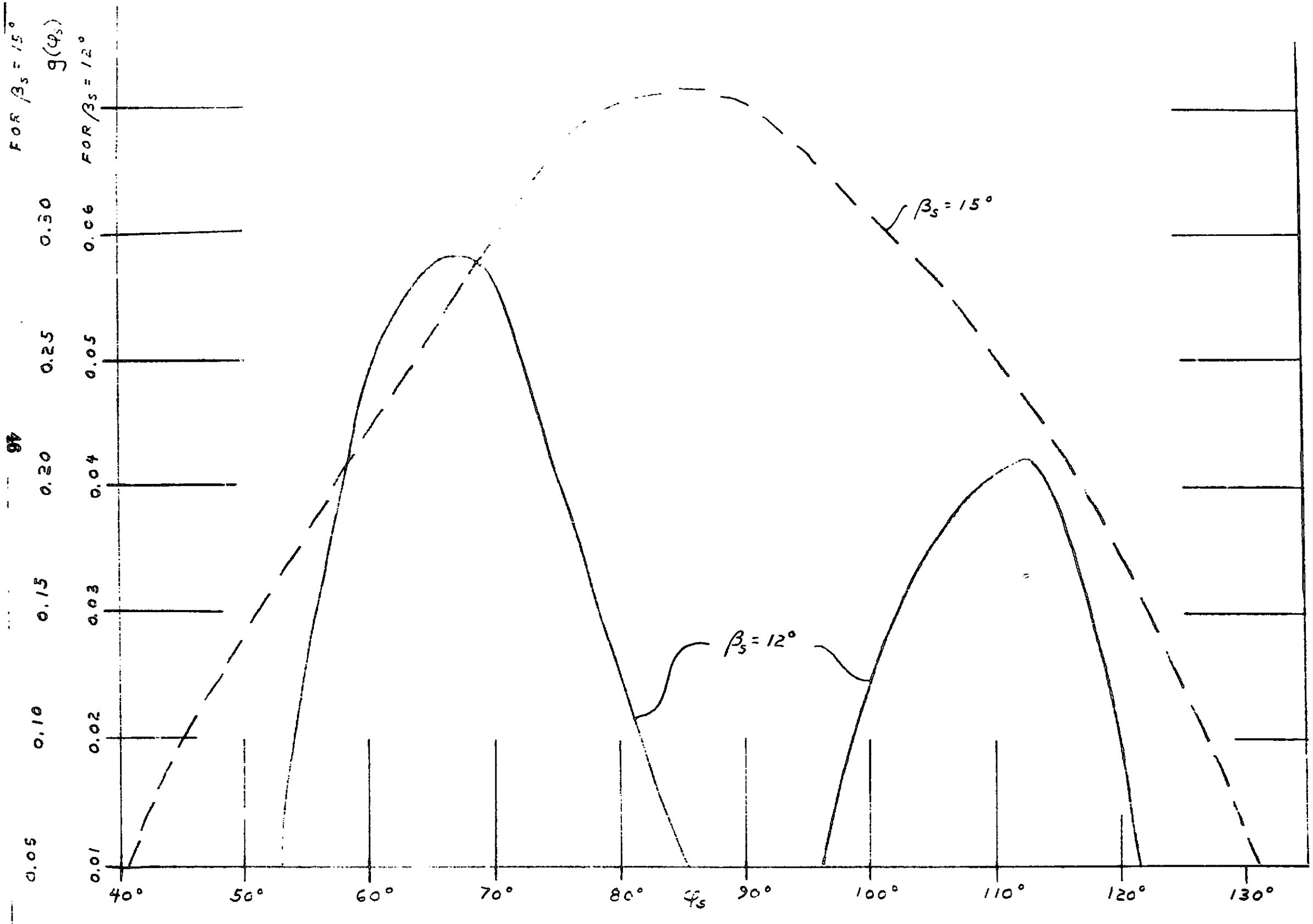

Figure 14 Cone End Exposure Factors (Design II)

Solar exposure of the cone mouth occurs at azimuth angles from 47 degrees to 69.5 degrees and from 110 degrees to 121 degrees over the range from 0 degrees to 180 degrees. During exposure of the cone mouth, either one or two cone wall reflections are needed for a solar ray to be reflected back out the cone mouth. We, therefore, need to determine the average cone mouth solar exposure factors g_n for one and two cone wall reflections.

The maximum values of $g_n(\varphi_s)$ in the above ranges occur at azimuth angles of approximately 60 degrees and 115 degrees. We will therefore approximate the integrals for g_n by

$$g_n = 1/\pi \int_0^{\pi} g_n(\varphi_s) \cdot d\varphi_s \doteq \frac{22.5^o}{180^o} \times \frac{1}{2} g_n(60^o) + \frac{11^o}{180^o} \times \frac{1}{2} g_n(115^o)$$

This assumes that the average value of $g_n(\varphi_s)$ over an azimuth angle range in which it is not equal to zero is one-half its maximum value in that range.

The values of $g_n(\varphi_s)$ at 60 degrees and 115 degrees were determined by projecting the cone mouth and two of its first reflection images (formed by specular reflection in the cone walls) into a plane perpendicular to the solar rays. The shadow cast over the cone mouth by the shield is projected into the same plane to determine the projected cone mouth area exposed to direct sunlight. These projections are shown in Figures 15 and 16 for a sun elevation angle β_s of 15 degrees. The necessary equations are derived in Appendix IV.

The parallelogram 2a' x 2b' shown in Figures 15 and 16 is the projection of the cone mouth rectangle 2a x 2b. The lines ℓ_1, ℓ_2, and ℓ_3 are the boundaries of the projections of the single reflection cone mouth images visible to the solar rays. They divide the projected cone mouth area into regions in which either one or two cone wall reflections are needed for a solar ray to be reflected back out the cone mouth. The projected shadow cast by the shield limits the exposed cone mouth areas to the corners (See also Figure 13.)

We obtain the required exposure factors from

$$g_n(\varphi_s) = \frac{A_N(\varphi_s)}{4ab \cdot \sin\beta_s} \qquad (36)$$

where $A_N(\varphi_s)$ is the projected cone mouth area over which incident sunlight requires N cone wall reflections to leave the cone. From Figures 15 and 16, we obtain

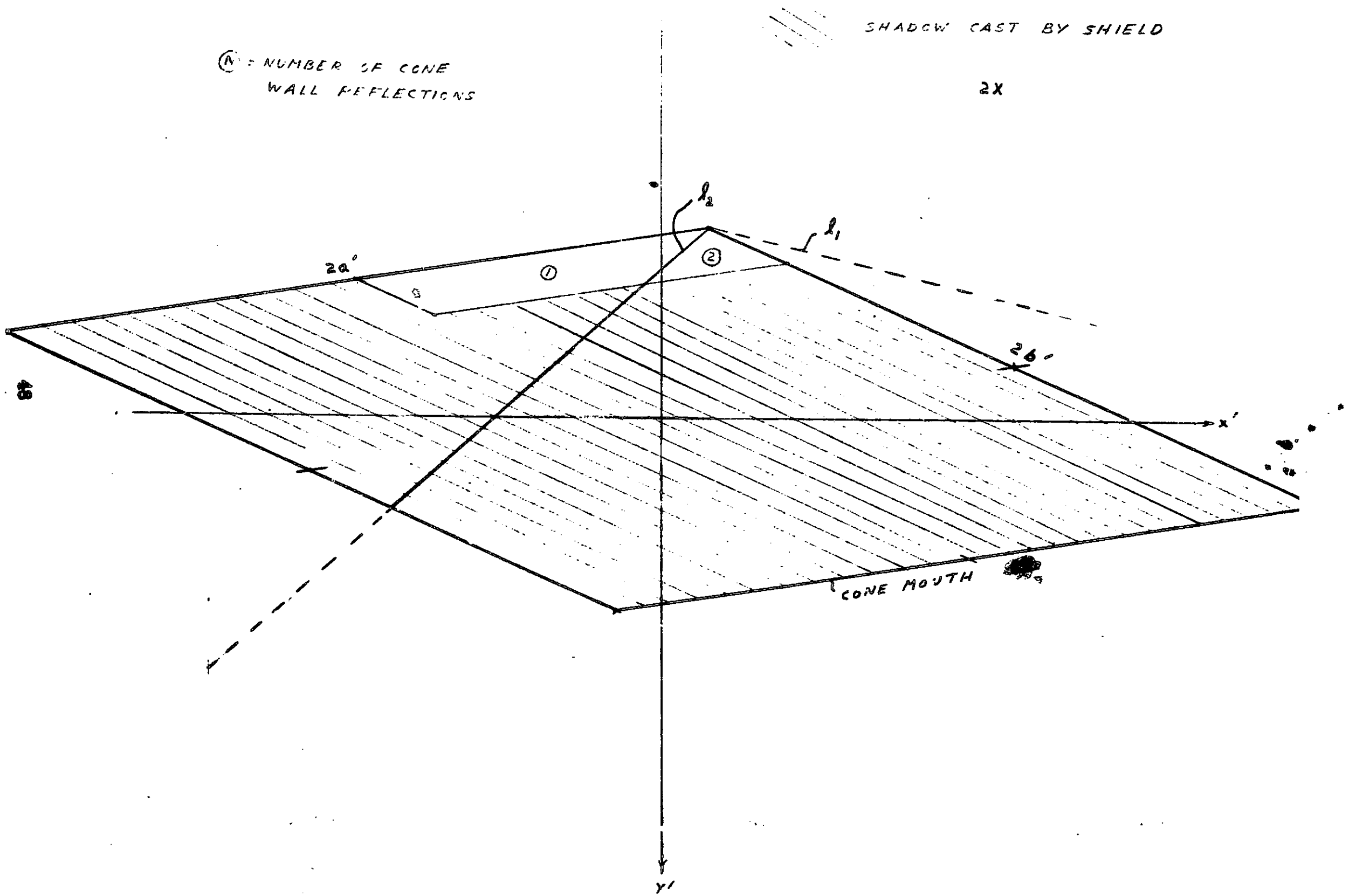

Figure 15 Cone Mouth and Images in Plane Perpendicular to Solar Rays at $\varphi_s = 60^o$ and $\beta_s = 15^o$ (Design II)

SHADOW CAST BY SHIELD

2x

(N) = NUMBER OF CONE WALL REFLECTIONS

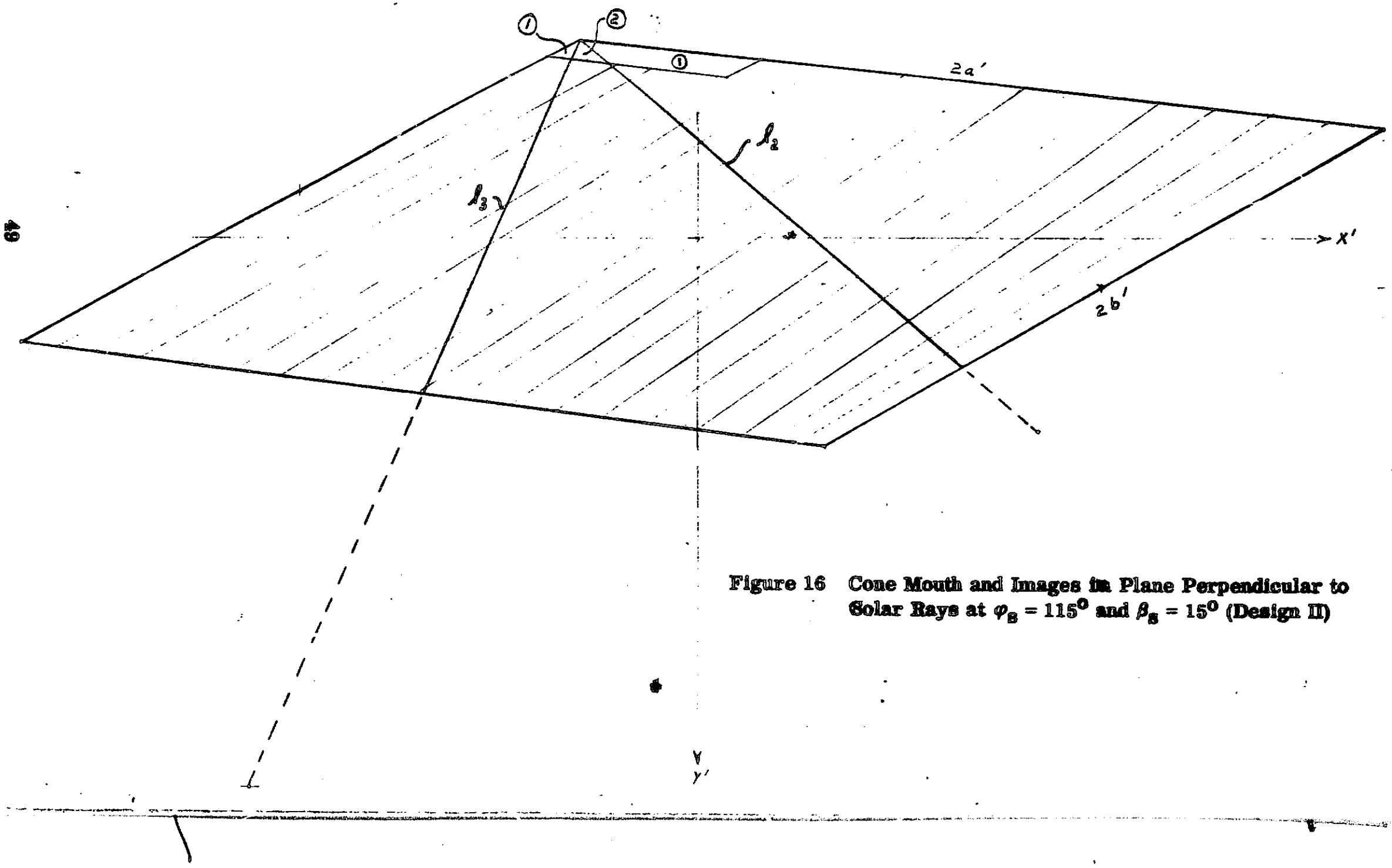

Figure 16 Cone Mouth and Images in Plane Perpendicular to Solar Rays at $\varphi_s = 115^o$ and $\beta_s = 15^o$ (Design II)

$$g_1\,(60^{\circ}) = 0.064, \qquad g_1\,(115^{\circ}) = 0.022,$$

$$g_2\,(60^{\circ}) = 0.014, \qquad g_2\,(115^{\circ}) = 0.0015.$$

The average solar exposure factors are then

$$g_1 = 4.7 \times 10^{-3},$$

$$g_2 = 9.2 \times 10^{-4}.$$

7.0 NEW TECHNOLOGY

The design of the single stage radiant cooler described in this report utilizes new technology developed on Contract No. NAS5-10113 (see Section 8.0). Specific technology utilized are the patch supports, patch optical opening, and earth shield. The single-ended cooler permits the addition of multilayer insulation to the sides of the patch with a further improvement in the thermal design of the patch optical opening (Appendix I).

8.0 BIBLIOGRAPHY

1. Final Report for a Day-Night High Resolution Infrared Radiometer Employing Two-Stage Radiant Cooling, Part I, Contract No. NAS5-10113, ITT Industrial Laboratories for Goddard Space Flight Center, 11 December 1967.

   This report describes the design, thermal analysis, and testing of a two-stage, double-ended, radiant cooler. Space chamber experiments demonstrated the feasibility of attaining 80 K in a Nimbus orbit.

2. Report of the Study for the Design of the Very High Resolution Radiometer for the Improved TOS Spacecraft. Contract No. NAS5-10491, ITT Industrial Laboratories for Goddard Space Flight Center, April 1968.

   This report covers the design study of a very high resolution radiometer for use on the improved TOS spacecraft. It includes the mechanical and thermal design of a two-stage, single-ended radiant cooler.

   The breadboard model achieved a second-stage temperature between 85 K and 90 K (monthly reports for January, February, and March 1969).

3. First Quarterly (Design Study) Report for Infrared Filter Wedge Spectrometer Instrument for Nimbus D Satellite, Contract No. NAS5-10388, ITT Industrial Laboratories for Goddard Space Flight Center, 24 July 1967.

   This report covers the design study of a filter wedge spectrometer for the Nimbus spacecraft. The instrument contains a single-stage, single-ended radiant cooler that maintains a PbSe element at 175 K. Additional design details and space chamber test results are reported in subsequent quarterly reports (second through eighth).

4. Radiant Cooling, R. V. Annable, to be published in Applied Optics (January 1970).

   This article develops an approach to the design and analysis of passive radiant coolers, especially those of rectangular geometry. It includes a summary of radiant coolers employed in spacecraft instruments.

APPENDIX I

RADIATIVE INPUT THROUGH OPTICAL OPENINGS TO PATCH

The exact magnitude of the radiative input (Φ_0) to the patch through the optical openings depends on the particular instrument design. However, a realistic estimate can be made for a high resolution instrument in which certain design approaches are generally employed.

To maintain accurate positioning of the detector with respect to the optics, the last lens is mounted in the patch with the detector element. Use of an aplanatic lens in this position allows an increase in the speed of the optical beam by a factor equal to the refractive index of the lens material. Thus for a germanium element (refractive index of 4) and a final speed at the detector of f/0.9 to f/1.0, the speed of the beam striking the element is f/3.6 to f/4.0. This relatively low speed, in turn, generally allows placement of the spectral filter on the patch in front of the aplanatic lens without significantly changing its spectral characteristics (as a result of variations in the incidence angle). In this position, the interference filter reduces Φ_0 by reflecting an appreciable fraction of the radiation incident from the optics on the instrument housing and from the structure between the housing and patch.

In addition, the optical opening is designed so that it does not pass through the cone wall area seen by the black top of the patch (Figure I-1). The first structure seen from the patch is then the multilayer insulation between the patch and cone rather than that between the cone and housing. As a result, the source closest to the optical opening on the patch is at a lower temperature.

The value of Φ_0 may be estimated by assuming that an area A_0 of each of two spectral filters at the edge of the patch views black optics at the housing temperature and black multilayer insulation (seen edge on) between the patch and cone and between the cone and housing. We then have

$$\Phi_0 = 2\sigma A_0 \left(E_A F_{pA} T_A^4 + E_B F_{pB} T_B^4 + E_H F_{pH} T_H^4\right) ,$$

where E_j = fraction of blackbody radiation at a temperature T_j that is transmitted by the filter (the remainder being reflected)

F_{pj} = view factor from A_0 to area j

A = multilayer between patch and cone

B = multilayer between cone and housing

H = optics at housing temperature

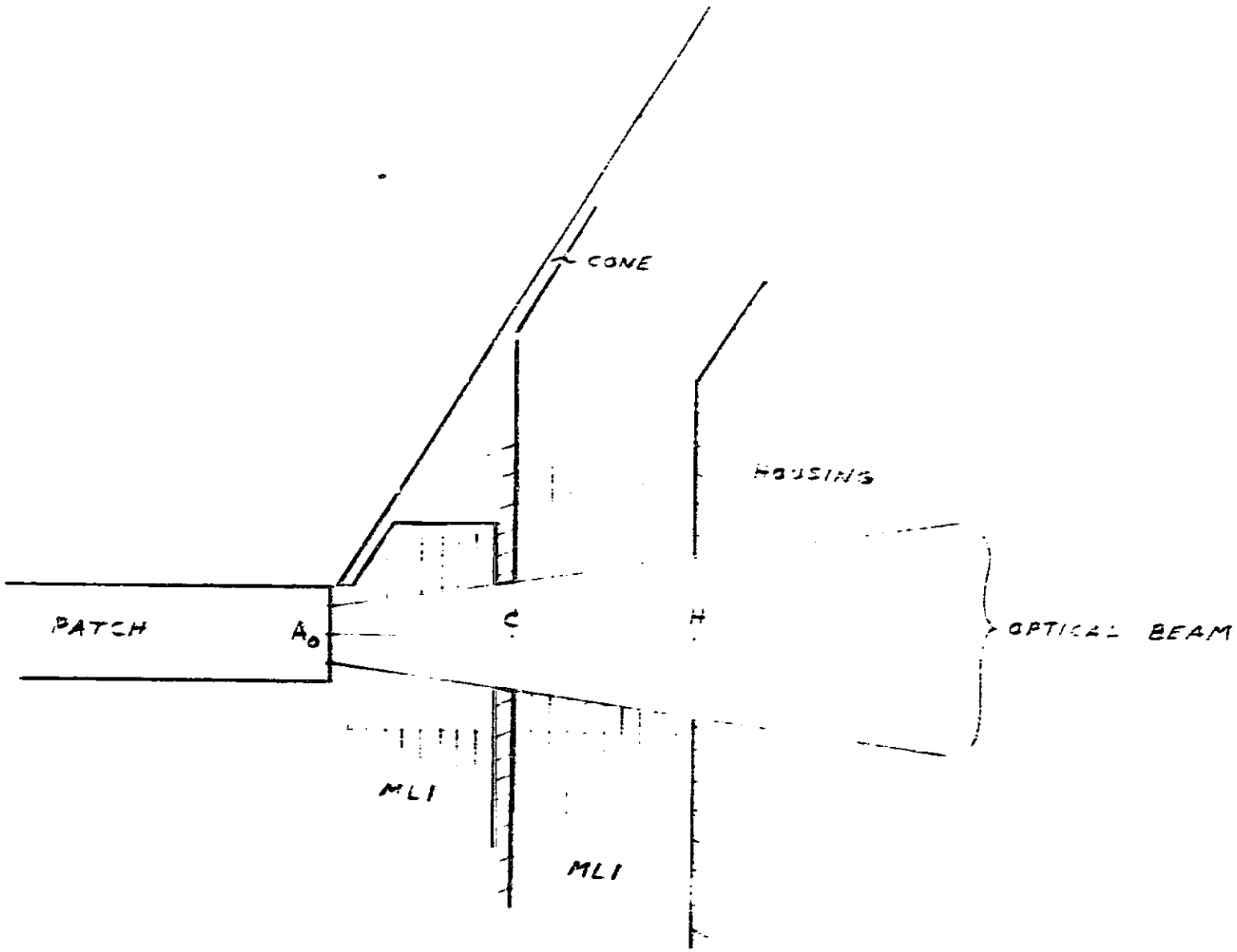

Figure I-1 Optical Opening Between Housing and Patch

The insulations are assumed to be at temperatures given by

$$T_A^4 = 1/2\,(T_c^4 + T_p^4) \cong 1/2\,T_c^4$$

$$T_B^4 = 1/2\,(T_c^4 + T_H^4)$$

In radiant cooler Design II, the opening between insulation blankets (i.e., in the cone structure) is 1 inch from the patch edge and 1 inch from the housing. The opening (A_o) at the edge of the patch is typically a circle whose diameter is in the range from 0.25 to 0.30 inch. We will assume that its diameter is 0.27 inch. The opening at the cone structure is then 0.55 inch in diameter for an f/3.6 beam between filter and housing and the opening at the housing about 0.83 inch in diameter. The three openings are circles with a common central normal. View factors between them may, therefore, be calculated from the formula given by M. Jakob (Heat Transfer, Vol. II, John Wiley and Sons, 1957, p. 14). The view factor to the housing, F_{pH}, is obtained this way. If F_{pC} is the view factor from A_o to the opening in the cone structure, the other two view factors are given by

$$F_{pA} = 1 - F_{pC}$$

$$F_{pB} = F_{pC} - F_{pH}$$

For the geometry described above, the results are

$$F_{pA} = 0.931$$

$$F_{pB} = 0.028$$

$$F_{pH} = 0.041$$

We will neglect the small fraction of radiation passed by the narrow spectral band to which a channel is sensitive. Instead, we will assume that all wavelengths greater than 18 microns (where the detector is insensitive) are transmitted by the filter. For $T_H = 308$ K and $T_c = 170$ K, $T_A = 143$ K and $T_B = 265$K (Design II). We then have the approximate values

$$E_A = 0.7$$

$$E_B = 0.4$$

$$E_H = 0.3$$

Finally, the radiative input through two optical channels is approximately

$$\Phi_o = 1.8 \times 10^{-3}\ \text{W}$$

APPENDIX II

EQUATION FOR EARTH'S HORIZON FROM A TILTED COOLER SURFACE

The geometry is shown in Figure II-1. The unit normal $\vec{n}_1$ to an elemental cooler area is tilted an angle α in the y-z plane above the horizontal. Its components are

$$\vec{n}_1 = (0, \cos\alpha, \sin\alpha).$$

A unit vector rotated an angle φ from the y-z plane and lying in the plane of the tilted area has components

$$\vec{\ell}_1 = (\sin\varphi, \cos\varphi \cdot \sin\alpha, -\cos\varphi \cdot \cos\alpha).$$

The unit vector $\vec{n}_2$ normal to plane P of $\vec{n}_1$ and $\vec{\ell}_2$ is then

$$\vec{n}_2 = \vec{\ell}_1 \times \vec{n}_1 = (\cos\varphi, -\sin\alpha \cdot \sin\varphi, \cos\alpha \cdot \sin\varphi) .$$

The unit vector $\vec{n}_3 = (0, 0, 1)$ is normal to the circular disk C bounded by the tangent lines to the earth. A vector $\vec{\ell}_2$ (not a unit vector) along the intersection of plane P and disk C is then

$$\vec{\ell}_2 = \vec{n}_3 \times \vec{n}_2 = (\sin\alpha \cdot \sin\varphi, \cos\varphi, 0) .$$

The angle ζ between $\vec{\ell}_2$ and the y axis is then

$$\tan\zeta = \sin\alpha \cdot \tan\varphi \quad . \tag{II-1}$$

And the intersection with the x axis (Figure II-2)

$$c = \sec\alpha \cdot \tan\varphi - \tan\alpha \cdot \tan\theta = \cos\alpha \cdot \tan\varphi .$$

Note that the altitude of the tilted element above the plane of disk C is taken as unity.

By the law of sines (Figure II-2)

$$\sin(\psi - \zeta) = c \cdot \sin(\pi/2 + \zeta) \cdot \cot\beta_e ,$$

$$\sin(\psi - \zeta) = \cos\alpha \cdot \cot\beta_e \cdot \tan\varphi \cdot \cos\zeta . \tag{II-2}$$

Equations (II-1) and (II-2) can be used to relate the azimuth angle φ in the plane of the tilted element with the azimuth angle ψ in the plane of disk C,

$$\sin(\psi - \zeta) = \sin\psi \cdot \cos\zeta - \cos\psi \cdot \sin\zeta = \cos\alpha \cdot \cot\beta_e \cdot \tan\varphi \cdot \cos\zeta ,$$

$$\sin\psi - \cos\psi \cdot \tan\zeta = \cos\alpha \cdot \cot\beta_e \cdot \tan\varphi .$$

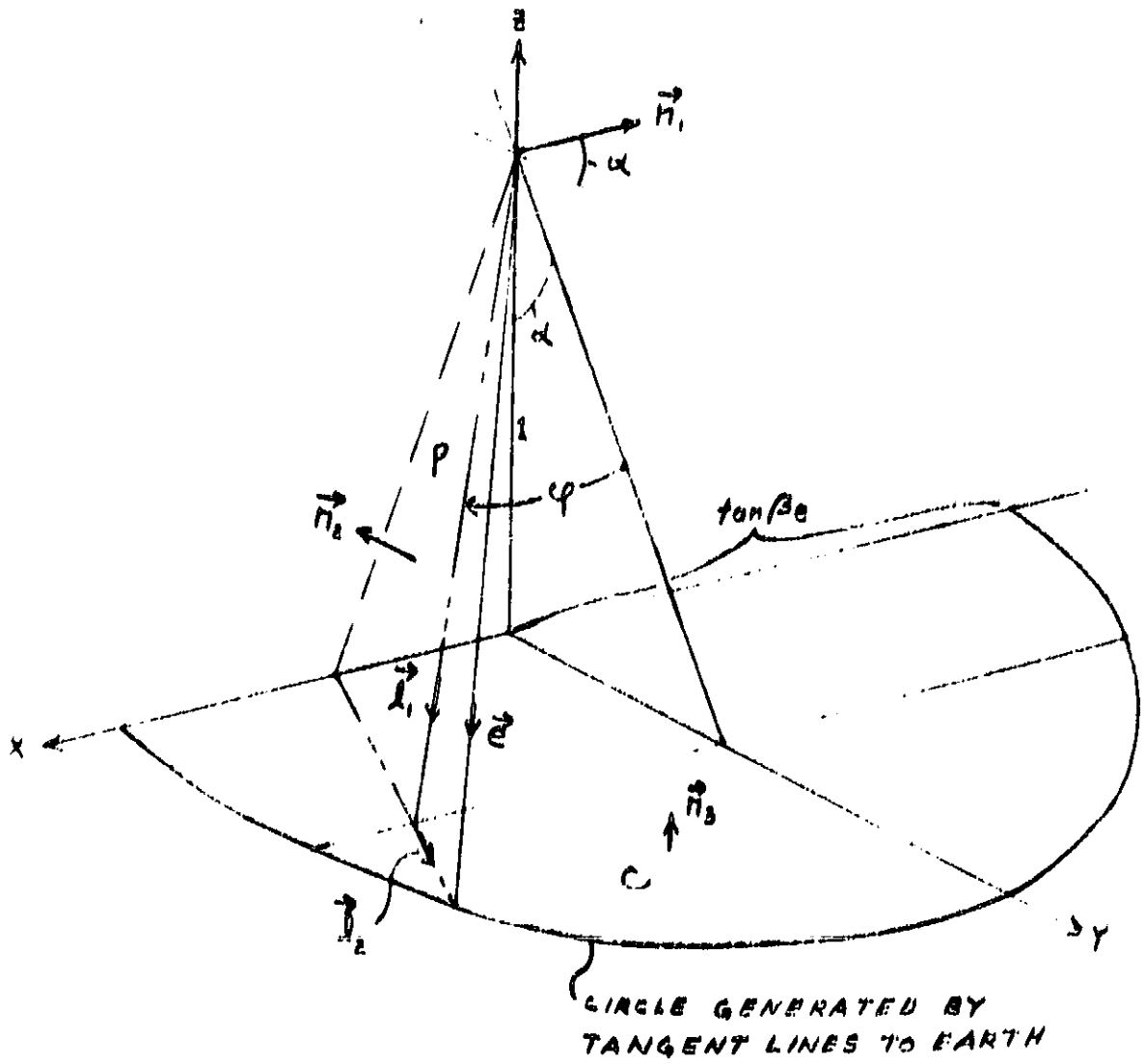

Figure II-1 Geometry of Earth's Horizon from Tilted Cooler Surfaces

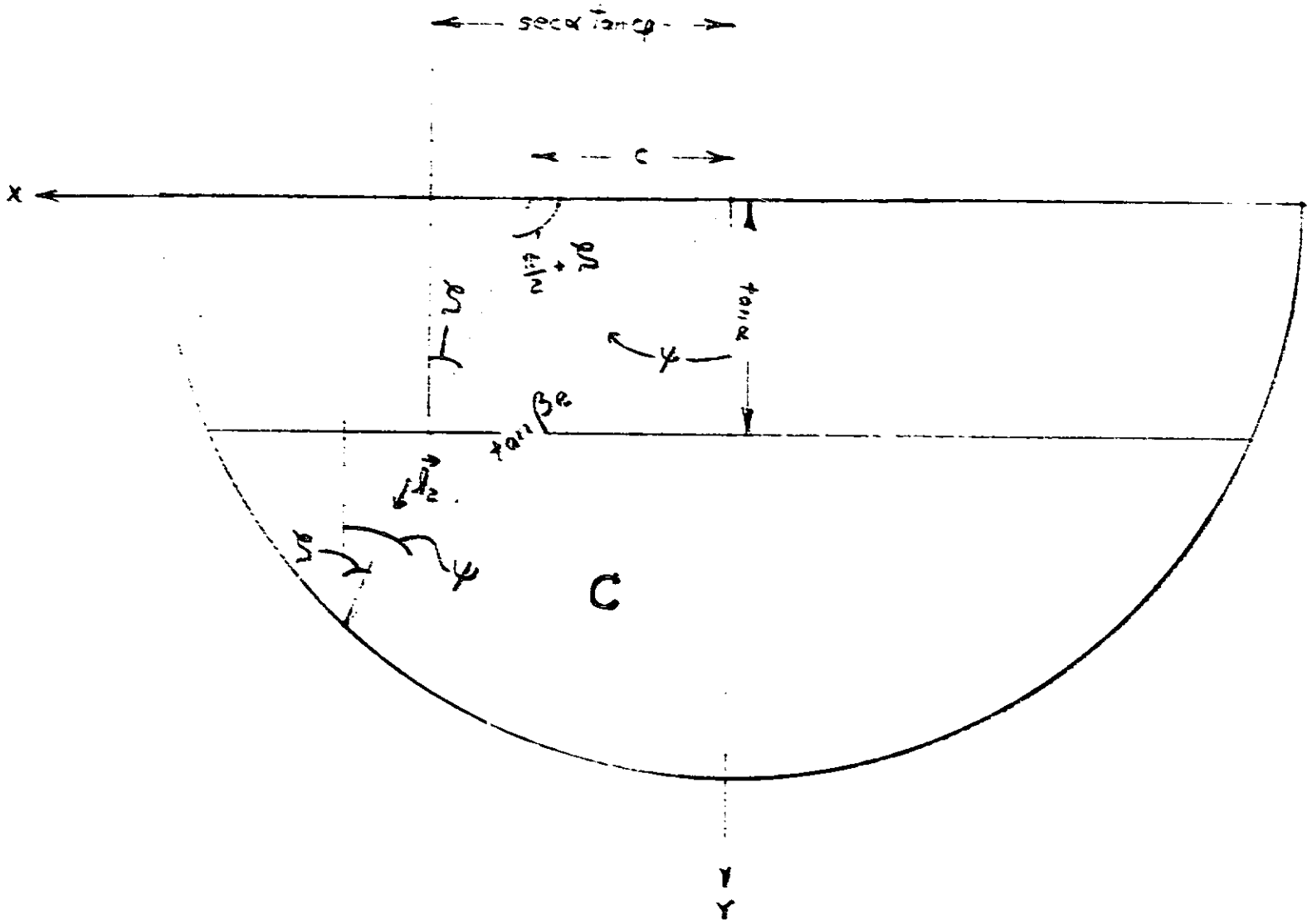

Figure II-2 Geometry in the Plane of Disk C

Solving for tan φ with the aid of Equation (II-1), we obtain

$$\tan \varphi = \frac{\sin \psi}{\cos \alpha \cdot \cot \beta_e + \sin \alpha \cdot \cos \psi} \quad . \qquad \text{(II-3)}$$

In order to calculate view factors from tilted cooler surface to the earth, we need the expression for

$$\sin^2 \vartheta_e (\varphi) \cdot d\varphi = \sin^2 \vartheta_e (\varphi) \cdot \frac{d\varphi}{d\psi} \cdot d\psi \qquad \text{(II-4)}$$

along the circle generated by tangent lines to the earth, where ϑ_e is the polar angle from $\vec{n}_1$. A unit vector along a straight line from the tilted element to the circle has components

$$\vec{e} = (\sin \beta_e \cdot \sin \psi, \quad \sin \beta_e \cdot \cos \psi, \quad -\cos \beta_e) \quad .$$

We then have

$$\sin^2 \vartheta_e = \left| \vec{n}_1 \times \vec{e} \right|^2 \quad ,$$

$$= \sin^2 \beta_e \left[(\cos \alpha \cdot \cot \beta_e + \sin \alpha \cdot \cos \psi)^2 + \sin^2 \psi \right] \quad , \qquad \text{(II-5)}$$

Differentiating Equation (II-3) yields

$$\frac{d\varphi}{d\psi} = \frac{\cos \alpha \cdot \cot \beta_e \cdot \cos \psi + \sin \alpha}{(\cos \alpha \cdot \cot \beta_e + \sin \alpha \cdot \cos \psi)^2 + \sin^2 \psi} \quad . \qquad \text{(II-6)}$$

Substituting (II-6) and (II-5) into (II -4), we obtain the desired equation

$$\sin^2 \vartheta_e (\varphi) \cdot d\varphi = \sin^2 \beta_e (\cos \alpha \cdot \cot \beta_e \cdot \cos \psi + \sin \alpha) \cdot d\psi \quad , \qquad \text{(II-7)}$$

where φ and ψ are related by Equation (II-3).

APPENDIX III

VIEW FACTOR FROM PATCH TO CONE MOUTH BY THREE CONE WALL REFLECTIONS (DESIGN II)

The cone mouth and its images formed by reflections in the cone walls fill the hemisphere above the patch. In cooler Design II, the hemisphere is filled by the cone mouth and its images formed by one and two reflections, except for two small identical triangular regions. These regions are bounded by the second reflection cone mouth image formed by reflection in the 10 degree wall followed by reflection in the 32 degree and 55 minutes wall, by the second reflection images formed by reflection in the 10 degree wall followed by reflections in 17 degree and 18 minutes walls, and by the extended plane of the patch (See Figure III-1).

The view factor to the two cone mouth regionsseen by three cone wall reflections from the patch is

$$F_{p-m\ (3)} = \frac{1}{\pi} \int_{\Delta} \sin^2 \vartheta\ (\varphi) \cdot d\varphi \ .$$

The first boundary is nearly perpendicular to the plane of the patch (actually at 85 degrees and 50 minutes). We will therefore assume that it is perpendicular, so that its equation is of the form φ = constant and it does not contribute to the above integral. We have then

$$F_{p-m\ (3)} = \frac{1}{\pi}\ (\varphi_b - \varphi_a) + \frac{1}{\pi} \int_{\varphi_b}^{\varphi_a} \sin^2 \vartheta_2\ (\varphi) \cdot d\varphi \ ,$$

where $\sin^2 \vartheta_2$ is the second boundary line running between azimuth angles φ_b and φ_a (Figure III-1). The second integral may be approximated by using the average value of $\sin^2 \vartheta_2$ between φ_a and φ_b,

$$I_2 = (\varphi_a - \varphi_b)(1/2)\left[1 + \sin^2 \vartheta_2\ (\varphi_a)\right] \ .$$

The view factor then becomes

$$F_{p-m\ (3)} = \frac{(\varphi_b - \varphi_a)}{2\pi} \left[1 - \sin^2 \vartheta\ (\varphi_a)\right] \ .$$

From the center of the patch in cooler design II to the triangular region in the first quadrant (Figure III-1),

$$\varphi_a = 31 \text{ degrees and } 3 \text{ minutes}$$

$$\varphi_b = 54 \text{ degrees and } 50 \text{ minutes}$$

$$\sin^2 \vartheta\ (\varphi_a) = 0.1036$$

and the view factor is approximately

$$F_{p-m\ (3)} = 0.0068$$

Therefore, only about 0.7 percent of the rays from the patch require three cone wall reflections to reach cold space.

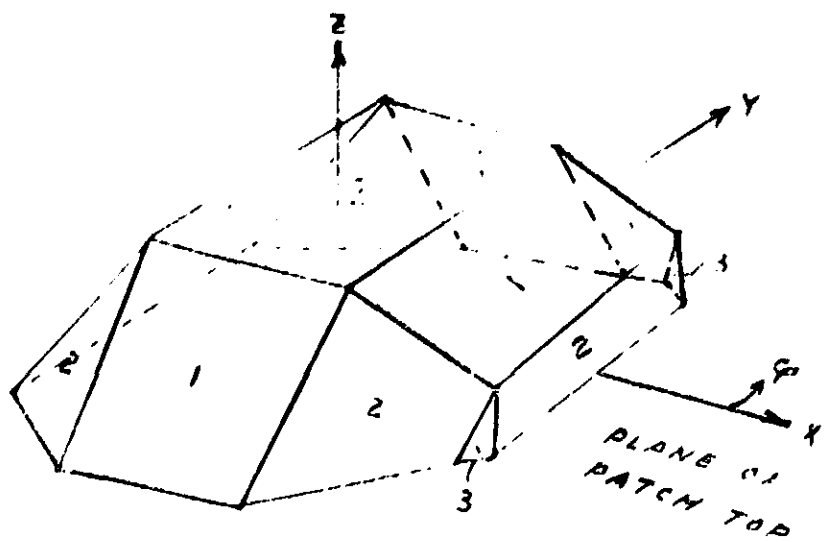

(a) Complete Array Above Patch

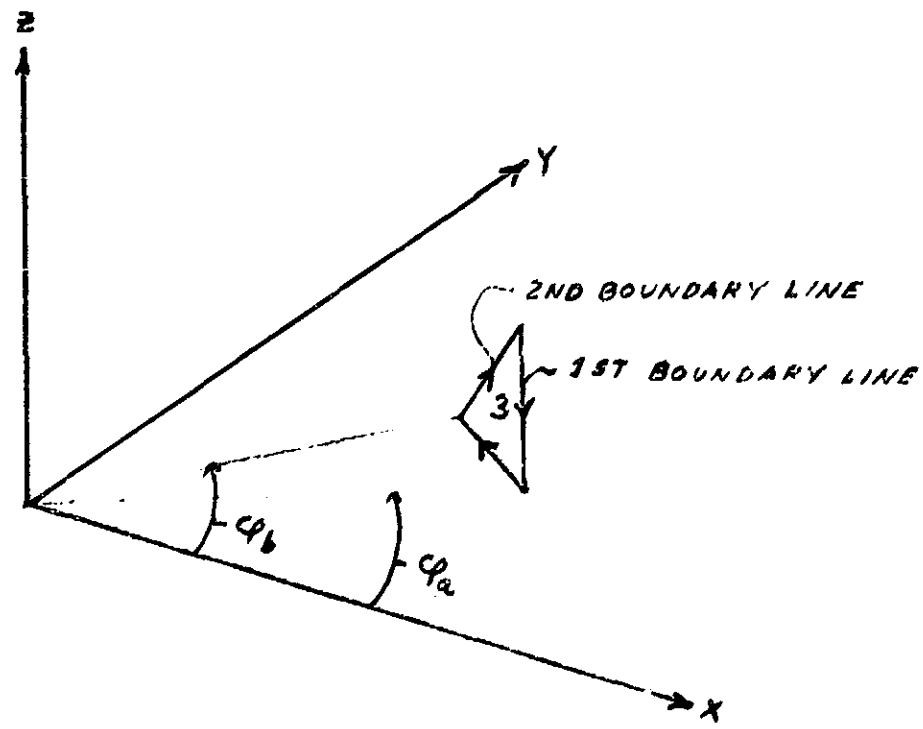

(b) Region of Three Reflections

Figure III-1 Cone Mouth Image Array

APPENDIX IV

PROJECTIONS OF CONE MOUTH AND ITS IMAGES IN A PLANE PERPENDICULAR TO SOLAR RAYS

Figure IV-1 shows a cartesian coordinate system (x y z) centered on the cone mouth. The half-sides of the cone mouth may be expressed as vectors

$$\vec{a} = (o,\ a,\ o)\ ,$$

$$\vec{b} = (b,\ o,\ o)$$

in this coordinate system. A solar ray incident at an azimuth angle φ_s (from the nadir y) in the x-y plane and an elevation angle βs above the x-y plane is shown in the same figure. This ray travels in the z' direction and is normal to the x' - y' plane.

Unit vectors along the axes in the (x' y' z') coordinate system have components in the (x y z) system given by

$$\vec{i'} = (-\cos\varphi_s,\ \sin\varphi_s,\ o)$$

$$\vec{j'} = (-\sin\varphi_s \cdot \sin\beta_s,\ -\cos\varphi_s \cdot \sin\beta_s,\ \cos\beta_s)$$

$$\vec{k'} = (\sin\varphi_s \cdot \cos\beta_s,\ \cos\varphi_s \cdot \cos\beta_s,\ \sin\beta_s)\ .$$

The projections of the vectors $\vec{a}$ and $\vec{b}$ (half-sides of the cone mouth) onto the x' - y' plane then have components given by

$$\begin{cases} x_a' = \vec{i'} \cdot \vec{a} = a \cdot \sin\varphi_s \\ y_a' = \vec{j'} \cdot \vec{a} = -a \cdot \cos\varphi_s \cdot \sin\beta_s \end{cases}$$

$$\begin{cases} x_b' = \vec{i'} \cdot \vec{b} = -b \cdot \cos\varphi_s \\ y_b' = \vec{j'} \cdot \vec{b} = -b \cdot \sin\varphi_s' \sin\beta_s \end{cases}\ .$$

Projections of the edges of the shadow cast by the cone shield can be found in a similar manner.

The vectors $\vec{\ell}_1$, $\vec{\ell}_2$, and $\vec{\ell}_3$ are, respectively, the reflections of $2\vec{a}$ in cone wall 1, of $2\vec{b}$ in cone wall 2, and of $2\vec{a}$ in cone wall 3. They are given by (for Design II)

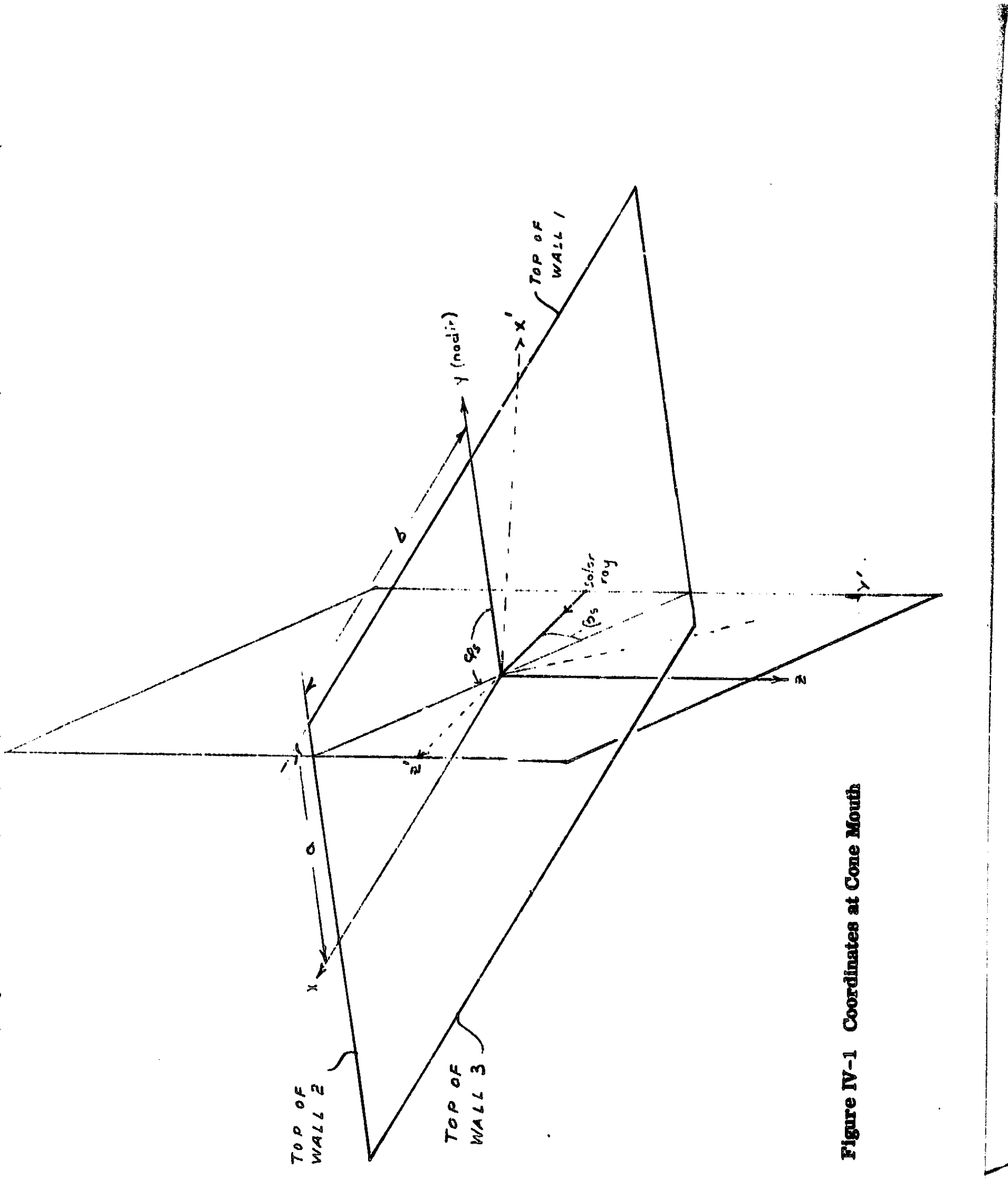

Figure IV-1 Coordinates at Cone Mouth

$$\vec{\ell}_1 = 2a\ (0\ ,\ \cos 20^o,\ \sin 20^o)$$

$$\vec{\ell}_2 = 2b\ (\cos 34^o\ 36',\ 0,\ \sin 34^o\ 36')$$

$$\vec{\ell}_3 = 2a\ (\ 0\ ,\ -\cos 65^o\ 50',\ \sin 65^o\ 50')\ .$$

And their projections onto the x'-y' plane are

$$\begin{cases} x_1' = \vec{i}' \cdot \vec{\ell}_1 = 2a \cdot \sin\varphi_s \cdot \cos 20^o \\ y_1' = \vec{j}' \cdot \vec{\ell}_1 = 2a\ (-\cos\varphi s \cdot \sin\beta_s \cdot \cos 20^o + \cos\beta_s \cdot \sin 20^o) \end{cases}$$

$$\begin{cases} x_2' = -2b \cdot \cos\varphi_s \cdot \cos 34^o\ 36' \\ y_2' = 2b\ (-\sin\varphi_s \cdot \sin\beta_s \cdot \cos 34^o\ 36' + \cos\beta_s \cdot \sin 34^o\ 36') \end{cases}$$

$$\begin{cases} x_3' = -2a \cdot \sin\varphi_s \cdot \cos 65^o\ 50' \\ y_3' = 2a\ (\cos\varphi_s \cdot \sin\beta_s \cdot \cos 65^o\ 50' + \cos\beta_s \cdot \sin 65^o\ 50') \end{cases}\ .$$

The above give the magnitudes and directions of the projections in the x'-y' plane but not their placements. However, it is known that the furthest corner of the projection (as viewed along a solar ray) lies at $\vec{a}' + \vec{b}'$ and that the projection of the cone mouth (a parallelogram) has sides 2a' x 2b'. Furthermore, the projection of any $\vec{\ell}$ vector which has one end at a given corner of the cone mouth is a vector $\vec{\ell}'$ which has the corresponding end at the projection of the same corner.